A Nanoparticle Carrying the p53 Gene Targets Tumors Including Cancer Stem Cells, Sensitizes Glioblastoma to Chemotherapy and Improves Survival

Sang-Soo Kim,[†] Antonina Rait,[†] Eric Kim,[‡] Kathleen F. Pirollo,[†] Maki Nishida,[‡] Natalia Farkas,[§] John A. Dagata,[§] and Esther H. Chang[†,*]

[†]Department of Oncology, Lombardi Comprehensive Cancer Center, Georgetown University, Washington, D. C. 20057, United States, [‡]SynerGene Therapeutics, Inc., Potomac, Maryland 20854, United States, and [§]National Institute of Standards and Technology, Gaithersburg, Maryland 20899, United States

ABSTRACT Temozolomide (TMZ)-resistance in glioblastoma multiforme (GBM) has been linked to upregulation of O^6-methylguanine-DNA methyltransferase (MGMT). Wild-type (wt) p53 was previously shown to down-modulate MGMT. However, p53 therapy for GBM is limited by lack of efficient delivery across the blood brain barrier (BBB). We have developed a systemic nanodelivery platform (scL) for tumor-specific targeting (primary and metastatic), which is currently in multiple clinical trials. This self-assembling nanocomplex is formed by simple mixing of the components in a defined order and a specific ratio. Here, we demonstrate that scL crosses the BBB and efficiently targets GBM, as well as cancer stem cells (CSCs), which have been implicated in recurrence and treatment resistance in many human cancers. Moreover, systemic delivery of scL-p53 down-modulates MGMT and induces apoptosis in intracranial GBM xenografts. The combination of scL-p53 and TMZ increased the antitumor efficacy of TMZ with enhanced survival benefit in a mouse model of highly TMZ-resistant GBM. scL-p53 also sensitized both CSCs and bulk tumor cells to TMZ, increasing apoptosis. These results suggest that combining scL-p53 with standard TMZ treatment could be a more effective therapy for GBM.

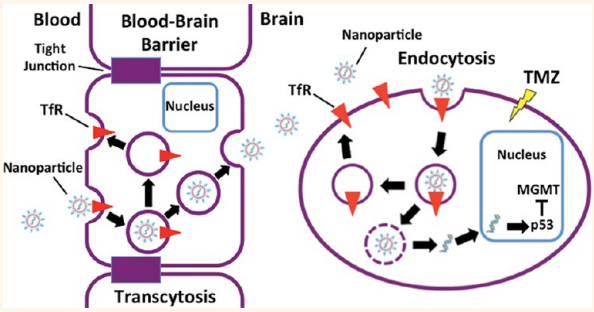

KEYWORDS: glioblastoma multiforme · crossing BBB · tumor/CSC targeting · p53 nanoparticle gene therapy · MGMT down-modulation · CSC apoptosis · chemosensitization

High-grade malignant glioma, glioblastoma multiforme (GBM), is the most aggressive and lethal form of brain tumor in adults.[1] Despite the intensive multimodal treatments comprising surgical resection and chemo/radiation therapy, the current prognosis of GBM patients remains poor in terms of length of survival (median survival of 14.6 months) and survival rate (below 4% for 5 year).[2,3] This dismal prognosis is mainly due to the high propensity of GBM to develop treatment resistance and to recur.[3] Cancer stem cells (CSCs) play a significant role in such resistance and recurrence. Furthermore, because of its extremely infiltrative nature, complete surgical resection of GBM is nearly impossible, inevitably leading to frequent tumor regrowth.

Temozolomide (TMZ), the current first-line chemotherapeutic agent for GBM, is an alkylating agent that generates cytotoxic DNA lesions. TMZ-induced O^6-methylguanine DNA adducts, if not removed by the DNA repair system, mispair with thymine, triggering rounds of futile mismatch repair which results in cell cycle arrest and ultimately apoptosis.[4] Although concurrent TMZ and radiation therapy has demonstrated a survival benefit, median survival is extended by only 2.5 months compared to radiation therapy alone.[5] Moreover, it has been reported that 60−75% of GBM patients do not benefit from TMZ treatment because GBM tumors are irresponsive or resistant to TMZ.[5] Thus, there is a critical need for means to overcome this drug resistance and expand the limited therapeutic benefit of TMZ.

* Address correspondence to change@georgetown.edu.

Received for review November 21, 2013 and accepted May 8, 2014.

Published online May 08, 2014
10.1021/nn5014484

There is a considerable body of evidence linking an elevated level of O^6-methylguanine-DNA methyltransferase (MGMT) with increased TMZ-resistance in GBM tumors.[6,7] MGMT is a ubiquitous DNA repair enzyme that repairs the damage induced by TMZ treatment.[8] Therefore, a means to effectively down-modulate MGMT activity could be a key factor for overcoming TMZ-resistance. In this regard, there has been an attempt to inhibit MGMT activity by using O^6-benzylguanine (O^6-BG), a pseudosubstrate of MGMT, as a MGMT inhibitor.[9,10] Although O^6-BG enhanced TMZ cytotoxicity in MGMT-proficient glioma cells,[11] the systemic coadministration of O^6-BG with TMZ in human patients resulted in serious myelotoxicity. In an effort to reduce this toxicity the dose of TMZ was reduced to a subtherapeutic level; however, none of the patients responded to this modified drug combination.[9,12]

The tumor suppressor gene p53 is frequently mutated (in ~30 and ~65% of primary and secondary GBM tumors, respectively)[13−15] and its signaling pathway is often compromised in GBM, making it a potential therapeutic target. In addition, p53 is of interest because MGMT expression is negatively regulated by wtp53 in cancer cells.[16] Furthermore, overexpression of wtp53 has been shown to increase the sensitivity of cancer cells to TMZ *in vitro* and in *in vivo* preclinical studies.[8,17−19] These results suggest wtp53-mediated silencing of MGMT as a logical approach to improve the efficacy of the current TMZ-based therapy by reversing the chemoresistance.

However, before the potential of wtp53-mediated inhibition of MGMT, as a means to enhance TMZ-based chemotherapy can be assessed, it is necessary to have a safe and effective means to transport wtp53 across the blood-brain barrier (BBB) and deliver it selectively to brain tumors. We have previously developed a tumor-targeting immunoliposome nanocomplex (designated as scL) for systemic delivery of molecular medicines. This scL nanocomplex is formed by simple mixing of the components in a defined order and a specific ratio. In this nanocomplex, the payload is encapsulated within a cationic liposome, the surface of which is decorated with an antitransferrin receptor (TfR) single chain antibody fragment (scFv) designed to target tumor cells *via* the TfR, which is highly expressed on surface of tumor cells.

Once the tumor-targeting scL-nanocomplex encounters the tumor cell, and the TfRscFv targeting moiety binds to the TfRs on the surface of the cell, the scL nanocomplex is efficiently internalized *via* receptor-mediated endocytosis. This is a well established, efficient method of internalization into the cell wherein the Tf receptor cycles into acidic endosomes into the cell.[20] The scL nanocomplex specifically delivers various payloads, including plasmid DNA,[21−26] siRNA,[27,28] and small molecules,[29] to both primary and metastatic tumor cells *in vivo*. This scL platform technology is currently in human clinical trials for wtp53 gene therapy (scL-p53 also called SGT-53) has completed a phase Ia, and is now about to complete a phase Ib human clinical trial in patients with advanced, metastatic, solid tumors. SGT-53 has been shown to be well tolerated at the therapeutic doses tested, and has demonstrated anticancer effect. The adverse effects identified in these trials are mild and transient. They consist primarily of grade 1 and 2 fever, chills, hypotension and occasionally tachycardia.[30] The FDA has also approved a phase Ib/II trial of SGT-53 in combination with gemcitabine for treatment of pancreatic cancer. Moreover, as the TfR is elevated on the cerebral endothelium of the BBB to mediate brain iron uptake,[31] this nanodelivery system can cross the BBB by TfR-mediated transcytosis.

Although current anticancer therapies are effective during the initial phase of treatment, frequently there are recurrences. Such recurrences can often be metastatic and resistant to conventional therapies. Within a tumor, a small population of cells (CSCs) has stem cell-like properties allowing them to initiate and fuel tumor growth. CSCs have been implicated in recurrence and treatment resistance in many human cancers, including brain. Unfortunately, the majority of conventional cancer therapies, including hormonal, radiation, and chemotherapy, may not efficiently eliminate CSCs. We have previously shown that the scL nanocomplex can target and efficiently deliver the payload to both CSCs and differentiated bulk tumor cells in various mouse models of human tumors including subcutaneous xenografts, syngeneic, and chemically induced tumors.[32] We have also shown that systemic administration of scL-p53 was able to induce tumor growth inhibition, as well as apoptosis in both CSCs and bulk tumor cells, in subcutaneous colorectal cancer xenograft tumors.[32]

Previous studies of the mechanism of formation of the nanocomplex when transferrin (Tf) itself was the targeting moiety explored the structure, size, formation process, and structure−function relationships of the nanocomplex.[21] It was observed to have a highly compact structure, with a relatively uniform size of 50−90 nm, resembling a virus particle with a dense core enveloped by a membrane coated with Tf molecules spiking the surface.[21] On the basis of these observations, a multistep self-assembly process and Tf-facilitated DNA co-condensation model was proposed that may provide an explanation for the resultant nanosize of the complex. Previously, studies using scanning probe microscopy (SPM) were also performed on the scL nanocomplex carrying a different payload to obtain quantitative size measurements of the nanocomplex, and to investigate how variations in the formulation or self-assembly process impact the size, structure and functionality of the scL nanocomplex.[33] Monitoring changes in the size distribution, structure and function contributed to the understanding of the self-assembly

process for that scL nanocomplex, and led to optimization of the formulation. As referenced in Farkas *et al.*,[34] SPM has the capability for imaging under physiological conditions. Taking advantage of this capability, there have been a number of studies that combine dynamic light scattering (DLS) size measurements with SPM characterization.[35−40] These studies have focused on characterization of soft biomaterials. The combination of fluid SPM and DLS size measurements has been reported to evaluate liposome rigidity and its dependence on size, cholesterol content, and phospholipid type.[37]

Here we show the results of additional SPM studies on the formation of scL-p53. In this study, we also evaluated whether this systemically administered tumor-targeting nanocomplex could target and efficiently deliver a fluorescence-labeled oligonucleotide (ODN) to GBM tumor CSCs in the brain. We also determined if efficient scL delivery of wtp53 plasmid DNA to intracranial GBM tumors after systemic administration could down-modulate MGMT expression and if such down-modulation would increase the response to TMZ of GBM tumors derived from highly aggressive, TMZ-resistant GBM cells resulting in enhanced survival.

RESULTS

Atomic Force Microscopy (AFM) Monitored Self-Assembly of scL-p53 Nanocomplex. At each stage of scL-p53 nanocomplex formation, AFM and DLS studies were performed. Because of the charge difference between the freshly cleaved mica substrate and the cationic liposomal nanocomplex, the nanocomplex may if weakly bound remain intact (see Figure S1, Supporting Information), or if strongly bound, rupture on contact with the substrate forming circular lipid patches. These lipid patches were found to provide a quantitative estimate of particle size by AFM. Fluid AFM was used to image both intact, as well as ruptured, liposomal complexes. Figure 1A shows representative AFM particle size distributions (in terms of an area-equivalent patch diameter) of the various stages of scL-p53 nanocomplex assembly: Liposome only (Lip), Liposome after mixing with TfRscFv to form scL, and the final full scL-p53 nanocomplex after mixing of scL with p53 plasmid DNA. The size distribution increases due to sequential reorganization of the lipid, first, through association with the TfRscFv targeting protein, and, second, with p53 plasmid DNA to complete the formation of the full complex. AFM images of such circular patches of Lip, scL and scL-p53 remaining after rupture of the particles are shown in Figure 1A. The average size distribution (measured by AFM) and zeta potential (ZP) (measured by DLS) of the complex at each stage in formation is also shown in Figure 1A. The size values of 37 $\pm$ 7 nm, 80 $\pm$ 18 nm and 101 $\pm$ 27 nm (Lip, scL, and scL-p53, respectively) indicate a modest increase at each stage in complex formation but clearly remain in the nanosize range, a finding similar to that observed when Tf was the targeting ligand in the nanocomplex.[21] Furthermore, after converting intensity-weighted DLS size distributions into number-weighted distributions and AFM distribution data to an equivalent spherical diameter, both methods yielded consistent sizes as previously reported by us.[34]

The ZP measured at each stage of complex was a positive value. Conjugation is not employed during scL-nanocomplex formation. The TfRscFv targeting moiety associates with the cationic liposome through a noncovalent charge−charge interaction. Thus, it is not unexpected that the ZP decreases with the addition of the TfRscFv, masking some of the surface charge on the liposome. In the same vein, encapsulation of negatively charged plasmid DNA by the liposome further decreases the positive charge of the nanocomplex. Significantly, the change in ZP for each stage of formation given in Figure 1A mirrors that observed in the earlier studies with TfL-p53.[21] TfL-p53 nanocomplex is composed of the identical liposome and wtp53 payload as scL-p53, but carries Tf itself on the surface of the liposome instead of the TfRscFv antibody fragment. The two nanocomplexes are prepared using the identical methodology.

AFM was also used to image the intact scL-p53 nanocomplex after absorption onto a UV/ozone treated poly-L-lysine coated mica (PLL-mica) substrate prepared as described in the Materials and Methods. The resulting image of the scL nanocomplex after drying is shown in Figure 1B (scL-p53, right panel). A previously published cryoEM of the TfL-p53 nanocomplex[21] (Figure 1B, left panel) shows the ultrastructure of this similar nanoparticle, which revealed a uniformly condensed core structure surrounded by a Tf-coated membrane. In fact, the presence of encapsulated plasmid DNA is clear in at least one particle (indicated by an arrow). Comparing the results shown here with the scL-p53 nanocomplex with the similar results published previously for TfL-p53[21] suggests that with simple mixing procedure, the formation for both nanoparticles could follow the same process.

Agarose gel electrophoresis was employed to assess the encapsulation (loading) efficiency of plasmid DNA in the scL nanocomplex (Figure 1C). Either 0.5 or 1 μg of plasmid DNA encoding wt human p53 was used in the preparation of the scL-p53 nanocomplex by simple mixing of the reagents. No separation or purification was performed after mixing. To detect unencapsulated plasmid DNA, the solution of nanocomplex was loaded onto a 0.6% agarose gel (lanes 1−3). The scL nanoparticle is too large to enter the gel and remains sequestered in the wells. Thus, only plasmid DNA remaining unencapsulated will move into the gel. To assess the amount of unencapsulated DNA, 5, 10, and 50 ng of free plasmid DNA was also loaded onto the gel. All three of these amounts of DNA (even the

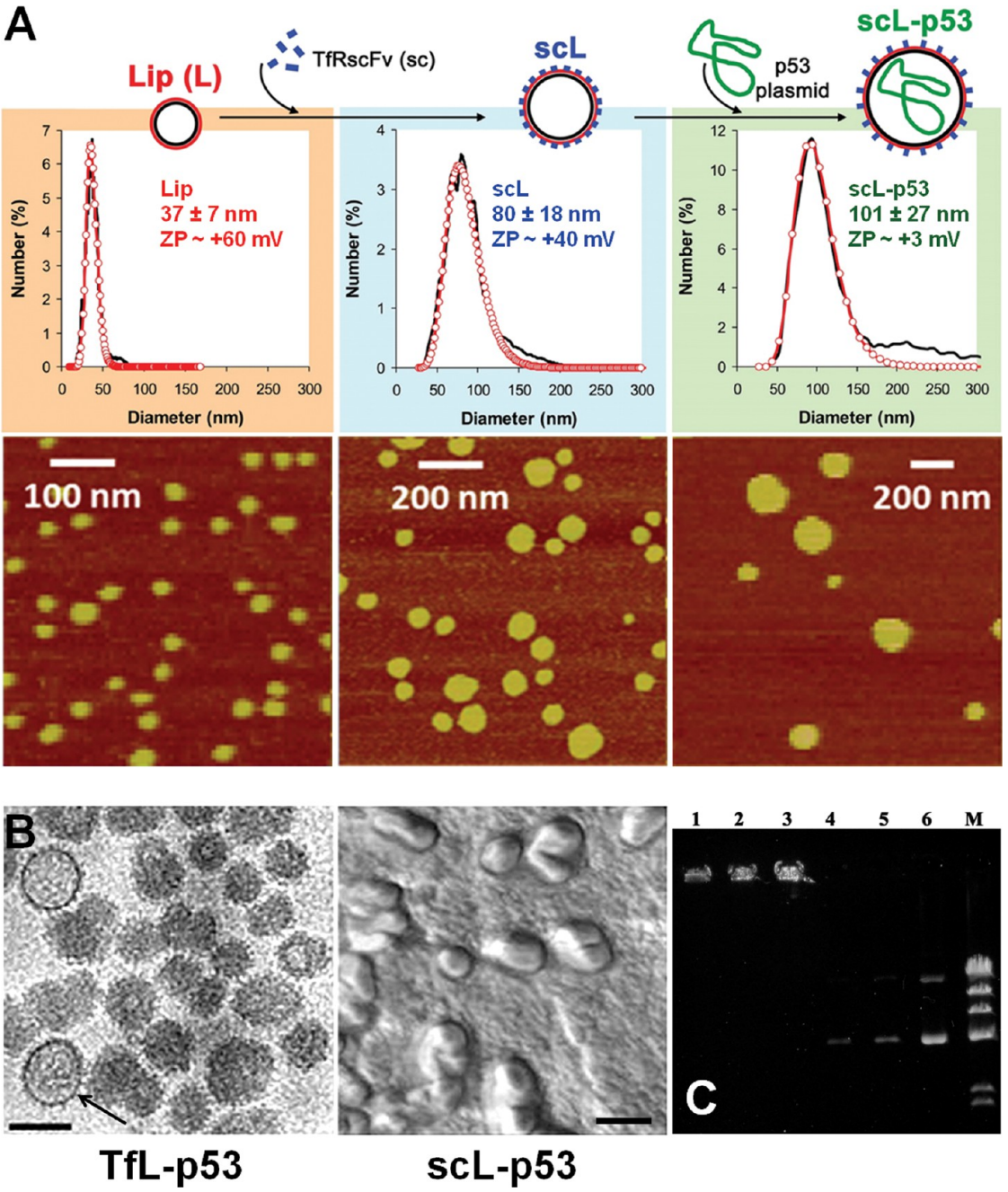

Figure 1. Self-assembly of scL-p53. After rupture of cationic liposomal complexes by contact with a negatively charged substrate, the resulting circular lipid patches were imaged by fluid AFM. (A) Size distribution of Liposome only (Lip), TfRscFv-Liposome (scL) and TfrscFv-Liposome-p53 plasmid DNA nanocomplex (scL-p53). Open circles represent a log-normal distribution fit to the multipoint averaged AFM data (upper panel). AFM images of circular patches of lipid remaining after rupture of liposomes and complex (lower panel). (B) CryoEM images of TfL-p53 (left panel) reprinted with permission from ref 21. Intact scL-p53 nanocomplexes adsorbed onto the substrate and imaged by AFM under dry conditions (right panel). Scale bars = 100 nm. (C) Agarose gel mobility shift assay to assess plasmid DNA encapsulation efficiency of the scL nanocomplex. Lanes 1−3 = scL-p53 nanocomplex prepared with p53 plasmid DNA at 0.5, 1.0, and 1.0 μg, respectively; lanes 4−6 = p53 plasmid DNA alone at 5, 10, and 50 ng, respectively; lane M = λ DNA/Hind III marker.

5 ng sample) were easily visualized by ethidium bromide (lanes 4−6). In contrast, in the lanes with the scL-p53 nanocomplex, there was no clear evidence of ≥5 ng of free plasmid DNA being present. Thus, this data shows that when prepared using the optimal ratio, > 99.5% of the plasmid DNA used in the preparation of the nanocomplex is encapsulated.

scL Nanocomplex Crosses the BBB and Targets CSCs *In Vivo*. As the goal of this study is to assess the potential of scL-p53 to sensitize tumor cells in the brain to chemotherapeutic TMZ, we initially performed a study to demonstrate the ability of the systemically administered scL nanocomplex to cross the BBB and deliver the payload to brain tumors. For these studies we employed fluorescently

(either Cy5- or 6FAM-) labeled ODN as a model payload. Mice bearing intracranial U87 GBM xenografts were injected intravenously (i.v.) once with either scL-Cy5-ODN, Lip-Cy5-ODN (the complex minus the targeting moiety), or free Cy5-ODN (all at 25 μg of Cy5-ODN/mouse/injection). 24 h after the injection, the fluorescence in the brain tumor and normal tissues (liver, kidney, and spleen) were imaged with the Maestro *in vivo* imaging system. The spectra was "unmixed", and the signal in each of the tumors was analyzed using the Maestro 2.10.0 software. The strongest fluorescence was observed in the intracranial tumors of mice injected with scL-Cy5-ODN (Figure 2A). In contrast, only weak fluorescence was detected in the intracranial tumors of mice treated with either untargeted Lip-Cy5-ODN or free Cy5-ODN. The quantitative measurements of the signal intensities in these tumors are shown in Figure 2B and correlate with the increase in color intensity in Figure 2A. Mirroring the results with the Maestro imaging, FACS analysis of Cy5-ODN uptake in cells isolated from these intracranial tumors showed that scL-mediated Cy5-ODN uptake, with an efficiency of 15.62%, was approximately 6 to 18 times greater than the uptake observed with the Lip-Cy5-ODN and free Cy5-ODN controls (2.64 and 0.87%, respectively) (Figure 2C, top panel). Further imaging of brain slices from one of the tumor-bearing mice treated with scL-Cy5-ODN in panel A (indicated by the *) showed a strong Cy5 signal

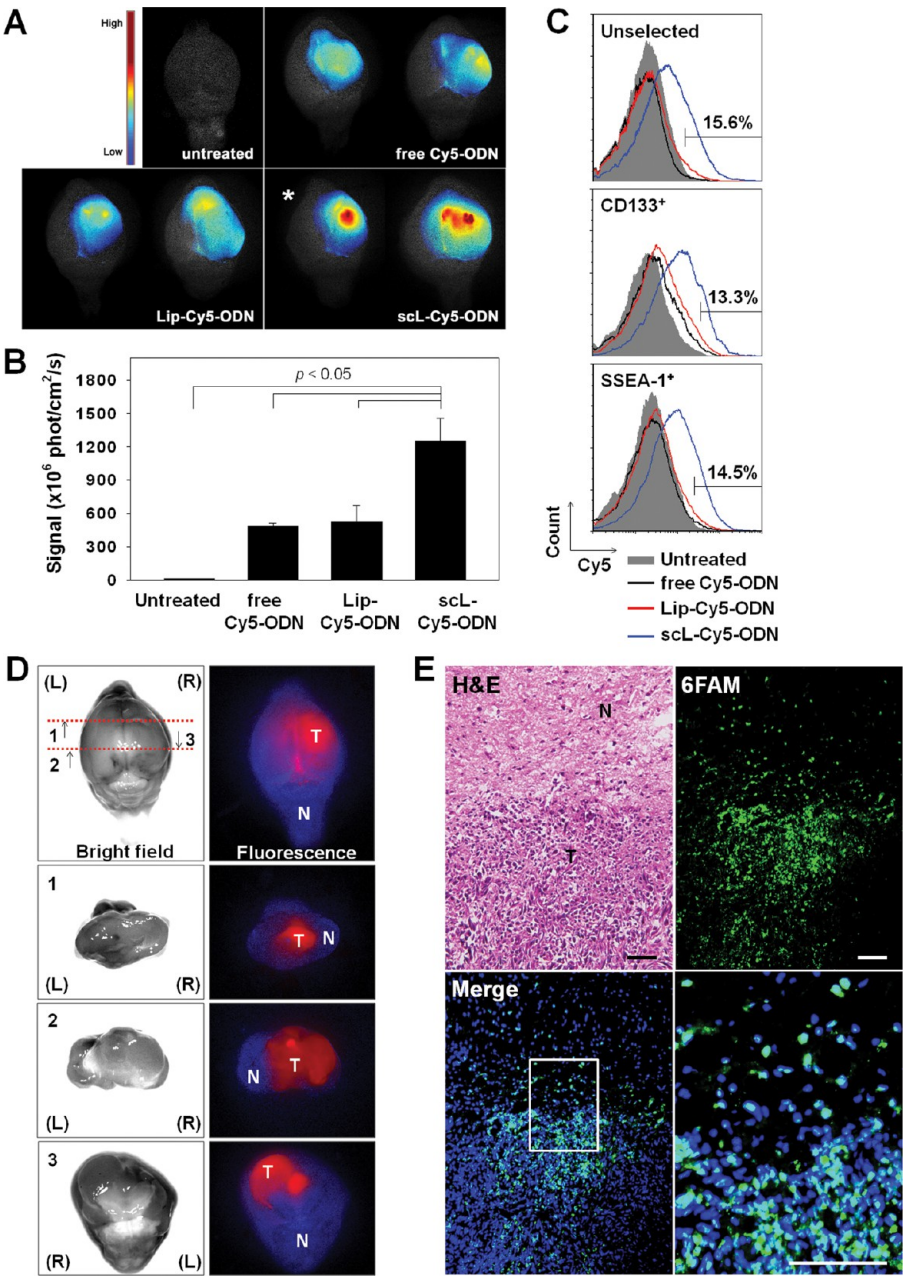

Figure 2. continued

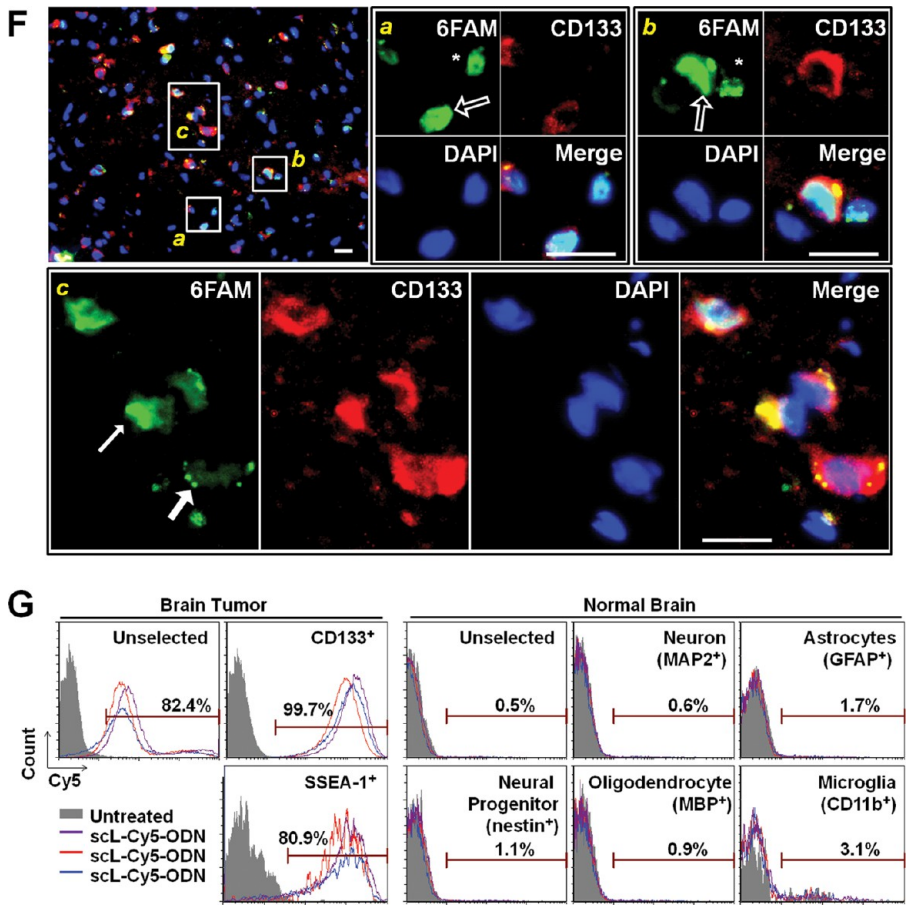

Figure 2. scL nanocomplex crosses the BBB. Mice with intracranially established U87 tumors were systemically injected with scL delivered ODN, fluorescently labeled with either Cy5- or 6FAM-, as a model payload to assess the targeting of brain tumors *in vivo*. (A) Representative images of brains bearing U87 tumors captured 24 h after a single i.v. injection with scL-Cy5-ODN (25 μg Cy5-ODN/mouse) using the Maestro *in vivo* fluorescence imaging system. The intensity of Cy5 fluorescence signal was shown in a color map. Dark red and blue colors indicate stronger and weaker fluorescence signals, respectively. Untreated, uncomplexed free Cy5-ODN, and unliganded Lip-Cy5-ODN served as controls. (B) Quantitative analysis of the intensity of Cy5 fluorescence signal, representing uptake of Cy5-ODN, in brain tumors using Maestro 2.10.0 software. Signal intensity is expressed as photons/cm^2/second. (C) FACS analysis of Cy5-ODN uptake in the tumor cells isolated from U87 tumors after imaging in A. Cy5-ODN uptake in unselected (top panel) and stem cell marker (CD133 and SSEA-1)-positive populations (center and bottom panels) was also analyzed by FACS. (D) Coronal slices of brain from mice treated with scL-Cy5-ODN in A (indicted by asterisk) were further imaged with Maestro. Blue: normal brain. Red: Cy5. N: normal brain. T: tumor. (E) Fluorescence images of an intracranial U87 tumor 24 h after a single i.v. injection with scL-6FAM-ODN (100 μg 6FAM-ODN/mouse). Tumor-bearing brain slices were stained with H&E (upper left) or DAPI. The DAPI stained slices were analyzed using confocal microscopy. High power image of the inset box in the merged image is shown on the right. Scale bars = 50 μm. (F) Tumor section described in E was further stained with an anti-CD133 antibody (red fluorescence) and analyzed using confocal microscopy. High power images of the inset boxes are shown (a, b, and c). Scale bars = 20 μm. (G) FACS analysis of Cy5-ODN uptake in the normal brain cells and tumor cells isolated from mice with established intracranial T98G tumors. Tissue was harvested 24 h after a single i.v. injection of scL-Cy5-ODN (25 μg Cy5-ODN/mouse). Cy5-ODN uptake in brain tumor cells (left panel) and normal brain cells (right panel) were analyzed by FACS.

detected specifically in the tumor and not in the normal brain tissue, demonstrating the tumor specificity of the scL-Cy5-ODN nanocomplex (Figure 2D).

CSCs have been implicated in recurrence and treatment resistance in many human cancers including brain tumors. Thus, here we assessed the ability of scL to target CSCs in intracranial xenograft tumors. In this study, two commonly used GBM CSC markers (CD133 and SSEA-1) were used to analyze Cy5-ODN uptake in CSCs by FACS. A single systemic injection of scL-Cy5-ODN resulted in an uptake efficiency of approximately 14% in both CD133$^+$ CSCs and SSEA-1$^+$ CSCs. In contrast, only approximately 1 and 2.5% of the CSCs showed the presence of the Cy5-ODN after i.v. injection of either free Cy5-ODN or untargeted Lip-Cy5-ODN (Figure 2C, middle and bottom panels).

The ability of systemically administered scL to deliver its payload across the BBB and target tumors was further evaluated *in vivo* using immunofluorescence analysis. Mice bearing intracranial U87 tumors received a single systemic (i.v.) injection with scL-6FAM-ODN at 100 μg of 6FAM-ODN/mouse. 24 h postinjection, using confocal microscopy, the localization of 6FAM (green fluorescence) was examined in

tumor-bearing brain sections stained with 4′,6-diamidino-2-phenylindole (DAPI) (Figure 2E). Abundant green fluorescence was observed in the brain tumor cells. H&E staining confirmed the margin of the tumor. It was also noted that there were a number of atypical cells beyond the tumor margin in the normal brain. A larger area of the H&E stained section with some of these cells indicated is shown in the Supporting Information as Figure S2. Nuclear colocalization of 6FAM-ODN and DAPI staining was also observed demonstrating the nuclear localization of the scL-delivered 6FAM-ODN payload.

The CSC-targeting capability of the scL nanocomplex *in vivo* was further confirmed by immunofluorescence analysis of tumor tissue using CSC marker CD133. The tumor sections described above were further stained with an anti-CD133 antibody (red fluorescence) and analyzed using confocal microscopy. As shown in Figure 2F, there is a strong green fluorescence signal evident in the cytoplasm of the cells (one example is indicated by a narrow arrow in Figure 2Fc). Confirming the results described above for Figure 2E, intense 6FAM fluorescence was also evident in the nucleus of many of the cells as indicated by the open arrows in Figure 2F, a and b. Nuclear localization was confirmed by colocalization with DAPI. More significantly, the red fluorescence signal indicative of CSC marker CD133 was found on the surface of many of the same cells containing the 6FAM green fluorescence signal in the cytoplasm and/or the nucleus.

Moreover, targeted scL delivery of the 6FAM-ODN was not limited to the CSCs, but was also evident in bulk tumor cells in the tumor. As shown in Figure 2F a and b, and indicated by the asterisk, there are cells exhibiting a high level of green fluorescence (specifically in the nucleus) but which do not colocalize with the red fluorescence signal of the anti-CD133 antibody. In some instances such cells are directly adjacent to CSCs showing that this lack of red fluorescence is not due to an artifact of the methodology.

One of the major challenges facing drug delivery by receptor-mediated endocytosis is ease of payload release from the endosomes. Cationic lipids destabilize the endosome membrane to facilitate the endosomal escape of nucleic acid such as plasmid DNA.[41] Cationic lipids form ion pairs with anionic lipids within endosome membrane to destabilize the endosome membrane. Because the cross-sectional area of the combined headgroup in the ion pair is less than that of the sum of individual headgroup areas alone, a "cylindrical" shape of individual charged lipids is transformed to a "cone" shape of ion pair that further promote the formation of the inverted hexagonal (HII) phase destabilizing the endosomal membrane resulting in release of the payload into the cytoplasm.[41]

The images in Figure 2F show cells at varying stages of uptake/release of the scL-6FAM-ODN in the tumor cells. An enlarged version of this figure is presented in the Supporting Information as Figure S3. The broad arrow in Figure 2Fc indicates early stage uptake with bright localized areas of fluorescence that, on the basis of the red CD133 surface signal, are located near the cell membrane. This possibly represents the complex just after endocytosis or within the endosomal pathway. However, in the same field are cells in which the green fluorescence is present in the cytoplasm (narrow arrow). It is important to note that in these cells the signal is dispersed throughout the entire cytoplasm. As the presence of the 6FAM-ODN payload still within the endosomes would result in a distinctive punctuate pattern of fluorescence within the cells, the observed diffuse distribution of the fluorescence indicates that the payload has been released from the endosomes. Furthermore, once in the cytoplasm the payload is now readily available to be transported into the nucleus, as is shown in many of the cells in Figure 2F, wherein the 6FAM-ODN fluorescence is localized in the nucleus (indicated by the open arrows in a and b). A previously published[32] *in vitro* time course, also demonstrating the scL nanocomplex moving from the endosomes to the cytoplasm and then to the nucleus, is presented in the Supporting Information as Figure S4. Thus, in addition to demonstrating CSC targeting, the above experiment also provides evidence that subsequent to receptor-mediated endocytosis of the scL nanocomplex, triggered by the binding of the TfRscFv targeting moiety to the TfR on the tumor cells, the payload is released from the endosomes into the cytoplasm and then into the nucleus.

To further test the tumor specificity of scL nanocomplex, Cy5-ODN uptake in various types of normal brain cells (*i.e.*, neurons, astrocytes and microglia) and brain tumor cells were compared by flow cytometry in mice bearing intracranial T98G GBM xenografts (Figure 2G). 24 h after a single i.v. injection of scL-Cy5-ODN (25 μg Cy5-ODN/mouse), FACS analysis of tumor cells and CSCs ($CD133^+$ and $SSEA\text{-}1^+$) isolated from these intracranial tumors showed significant uptake of Cy5-ODN with an efficiency of >80% (left panel). In contrast, no significant uptake of Cy5-ODN was observed in the normal brain cells (right panel). Only 3% of microglial cells were positive for Cy5-ODN, with the majority of other types at 1% or less.

Taken together, these results in mice bearing intracranial GBM xenograft tumors confirm not only the capability of the scL nanocomplex to cross the BBB, but also its tumor specificity and ability to target and efficiently deliver the payload into both CSCs and bulk tumor cells in the tumor after systemic administration.

scL-p53-Mediated Down-Modulation of Endogenous MGMT Expression in GBM cells *In Vitro* and *In Vivo*. To assess the effect of scL-delivered wtp53 on MGMT expression *in vitro*, MGMT-proficient T98G cells were transfected for 24 h with either scL-p53 or scL-vec (scL carrying the

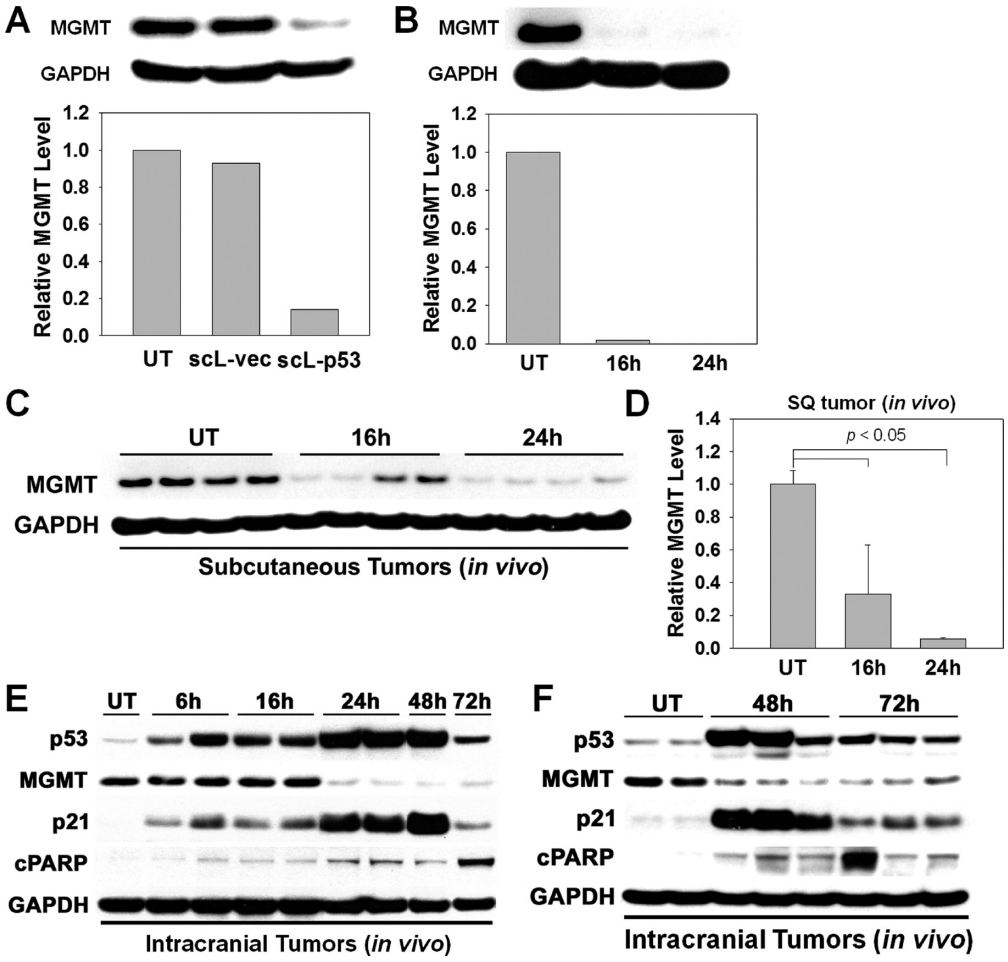

Figure 3. Time-dependent changes in expression of MGMT and p53 related proteins after the treatment with the scL-p53 nanocomplex *in vitro* and *in vivo*. *In vitro* studies: (A) Western blot analysis of MGMT and GAPDH protein levels at 24 h post-treatment of TMZ-resistant T98G cells with either scL-p53 or scL-vec (7 μg of DNA/dish) (upper panel). Densitometric quantification of the Western blot is shown in the lower panel in which MGMT expression is compared to that of the untreated (UT) control cells. (B) Western blot analysis of MGMT and GAPDH protein levels at 16 and 24 h after transfection of T98G cells with scL-p53 (7 μg of DNA/dish) (upper panel). Densitometric quantification of the Western blot is shown in the lower panel in which MGMT expression is compared to that of the untreated (UT) control cells. In both panels A and B, the lane in the Western blot corresponds to the bar directly below it. In both panels expression of GAPDH protein was utilized as an internal control for protein loading. *In vivo* studies: Mice with either subcutaneously or intracranially established T98G xenograft tumors were systemically (i.v. tail vein) injected with the scL-p53 nanocomplex (30 μg of DNA/mouse/injection). (C) Western blot analysis of MGMT and GAPDH protein levels in subcutaneous T98G xenograft tumors at 16 and 24 h after the last i.v. tail vein injection. (D) Densitometric quantification of the Western blot shown in C. (E, F) Western blot analysis of two independent experiments assessing changes in p53, MGMT, p21, and cleaved PARP protein levels in intracranial T98G xenograft tumors over time after the single i.v. tail vein injection. In both experiments expression of GAPDH protein was utilized as an internal control for protein loading.

empty vector) nanocomplex and monitored for changes in the MGMT protein level by Western blot analysis (Figure 3A). The mean particle size of scL-p53 in water was 114.4 $\pm$ 8.4 nm (number value). The mean zeta potential of scL-p53 was 28.2 $\pm$ 1.2 mV. Compared to the untreated T98G cells, there was a significant silencing of MGMT expression (~90% reduction) 24 h after treatment with scL-p53 nanocomplex (Figure 3A). In contrast, there was only no significant reduction of MGMT expression after transfection with the control scL-vec. The lack of MGMT down-regulation by scL-vec demonstrates that MGMT down-regulation is due to the presence of the exogenous p53 and a nonspecific effect of the TfRscFv-Liposome particle.

We also monitored the *in vitro* time-dependent changes in the MGMT protein level after treating T98G cells with scL-p53 nanocomplex (Figure 3B). Compared to the untreated T98G cells, there was almost complete silencing of MGMT expression by 16 h, which lasted at least to 24 h post-transfection.

We further examined the effect of scL-p53 on the expression of MGMT in two different animal xenograft models of GBM tumors: subcutaneous and intracranial. For mice bearing subcutaneous T98G xenografts, the scL-p53 nanocomplex (30 μg of DNA/injection/mouse equivalent to 1.5 mg/kg) was i.v. injected three times over a 24 h period. At 16 and 24 h after the last scL-p53 injection, tumors were harvested, and MGMT

expression was determined. Similar to the *in vitro* study above, a significant decrease in the expression of MGMT was evident by 16 h (~67% reduction), with virtual elimination of the protein in two out of four tumors (Figure 3C). By 24 h after the last injection, almost complete silencing of MGMT (~95% reduction) was evident in all of the mice treated with scL-p53 (Figure 3C, D).

More significantly, we also assessed MGMT down-modulation and the downstream response to scL delivered p53 in an intracranial mouse model of GBM. Mice bearing intracranial T98G tumors received a single i.v. tail vein injection of the scL-p53 nanocomplex (30 μg of DNA/mouse). At various times postinjection, the animals were sacrificed, and the tumors were examined for the level of expression of MGMT, p53, and other proteins in the downstream p53 signaling pathway. Relative to the level in the untreated tumor, a significant increase in the expression of p53 was observed as early as 6 h postinjection, which peaked at 48 h with a decreased level of expression by 72 h postinjection (Figure 3E). More importantly, a significant decrease in MGMT expression was observed, which inversely correlated with the expression of p53. A lag in the MGMT response to increasing levels of exogenous wtp53 protein was observed, with decreased MGMT not evident until 24 h. However, by 24 h, there was a virtually complete down-modulation of MGMT expression (~90% reduction), which was also observed until at least 72 h postinjection (Figure 3E). The densitometric quantification of the Western blot shown in Figure 3E is given in the Supporting Information as Figure S5. It should be noted that even at 72 h postinjection, p53 expression is still elevated relative to that observed in the untreated animals and is likely still contributing to the down-modulation of MGMT. The p21 (CIP1/WAF1) gene is a downstream effector of p53 and plays a crucial role in p53 signaling pathways. Thus, not unexpectedly, an increase in p21 expression was also observed. The timing of the increase in expression of both p53 and p21 was similar peaking at around 48 h postinjection. Moreover, expression of cleaved PARP, an indicator of apoptosis, was detected as early as 6 h and reached maximum expression 72 h postinjection (120-fold increase compared to untreated). This result was further confirmed in another, independent IC *in vivo* experiment which also assessed the level of expression of p53, MGMT, p21 and cleaved PARP at 48 and 72 h compared to those of untreated tumors (Figure 3F). The pattern and timing of the changes in expression the proteins tested in this second experiment mirrors the results of the initial study, confirming those findings (Figure 3E).

***In Vitro* Sensitization of GBM Cells to TMZ by the scL-p53 Nanocomplex.** To determine the effect of scL-p53-induced down-modulation of MGMT on the sensitivity of TMZ-resistant human GBM cells to TMZ *in vitro*, two different MGMT-proficient human GBM cell lines (LN-18 and T98G) were tested. 2×10^3 cells of each of the cell lines were plated/well of a 96 well plate 24 h prior to transfection.

Initially we assessed the response of these GBM cells to scL-p53, The XTT survival assay was performed 96 h after transfection of GBM cell lines LN-18 and T98G cells with increasing concentrations of the scL-p53, scL-vec nanocomplexes (0 to 250 ng/well, which is equivalent to 0 to 125 pg of DNA/cell) or the Lip alone. Transfection with scL-p53 resulted in a statistically significant increase in cell death in both cell lines. In contrast, transfection with the controls, at what would be clinically relevant doses and at the DNA dose used in the combination studies, did not result in significant cell death demonstrating that the response to scL-p53 is not a result of nonspecific cytotoxicity (Figure 4A,C).

To assess the ability of scL-p53 to sensitize GBM tumor cells to chemotherapeutics, LN-18 and T98G cells were transfected with scL-p53 (100 ng of DNA/well, which is equivalent to 50 pg of DNA/cell) for 24 h and then treated with increasing concentrations of TMZ (0 to 2500 μM) for an additional 72 h. Cells either treated with TMZ alone or transfected with the scL-vec were used as controls. Transfection with scL-p53 resulted in significantly increased response to TMZ in both of these TMZ-resistant cell lines. In contrast, without scL-p53 transfection, no significant cell death was observed in either cell line until a TMZ dose of at least 500 μM was reached. LN-18 cells are so sensitized by scL-p53 that they now respond to very low doses of TMZ (Figure 4B). Transfection with scL-p53 decreased the IC_{50} from 577 μM to 153 μM, almost 3.8-fold increase in sensitivity to TMZ. In contrast, there was minimal or no sensitization of the LN-18 cells to TMZ after transfection with the control scL-vec, again demonstrating that the response in these resistant cell lines is due to the presence of exogenous wtp53 and not nonspecific cytotoxicity. After treatment with scL-p53, the highly resistant T98G cells are also significantly sensitized to the killing effects of TMZ (Figure 4D). Transfection with scL-p53 decreased the IC_{50} from 742 μM to 210 μM, almost 3.5-fold increase in sensitivity to TMZ.

This chemosensitization by scL-p53 in MGMT-proficient T98G cells was also observed with another alkylating agent 1,3-Bis(2-chloroethyl)-1-nitrosourea (BCNU) (Figure 4E). The cells treated with scL-p53 (at a DNA dose of either 100 or 200 ng/well, which are equivalent to either 50 or 100 pg of DNA/cell, respectively) had a 10.1-fold and >54-fold increase, respectively, in response to BCNU. With these two DNA doses, the apparent IC_{50} value decreased from ~547 μM to either 54 or <10 μM, respectively. Thus, these results show the potential of this approach as a means of converting unresponsive tumors to tumors now responsive to these DNA alkylating chemotherapeutic

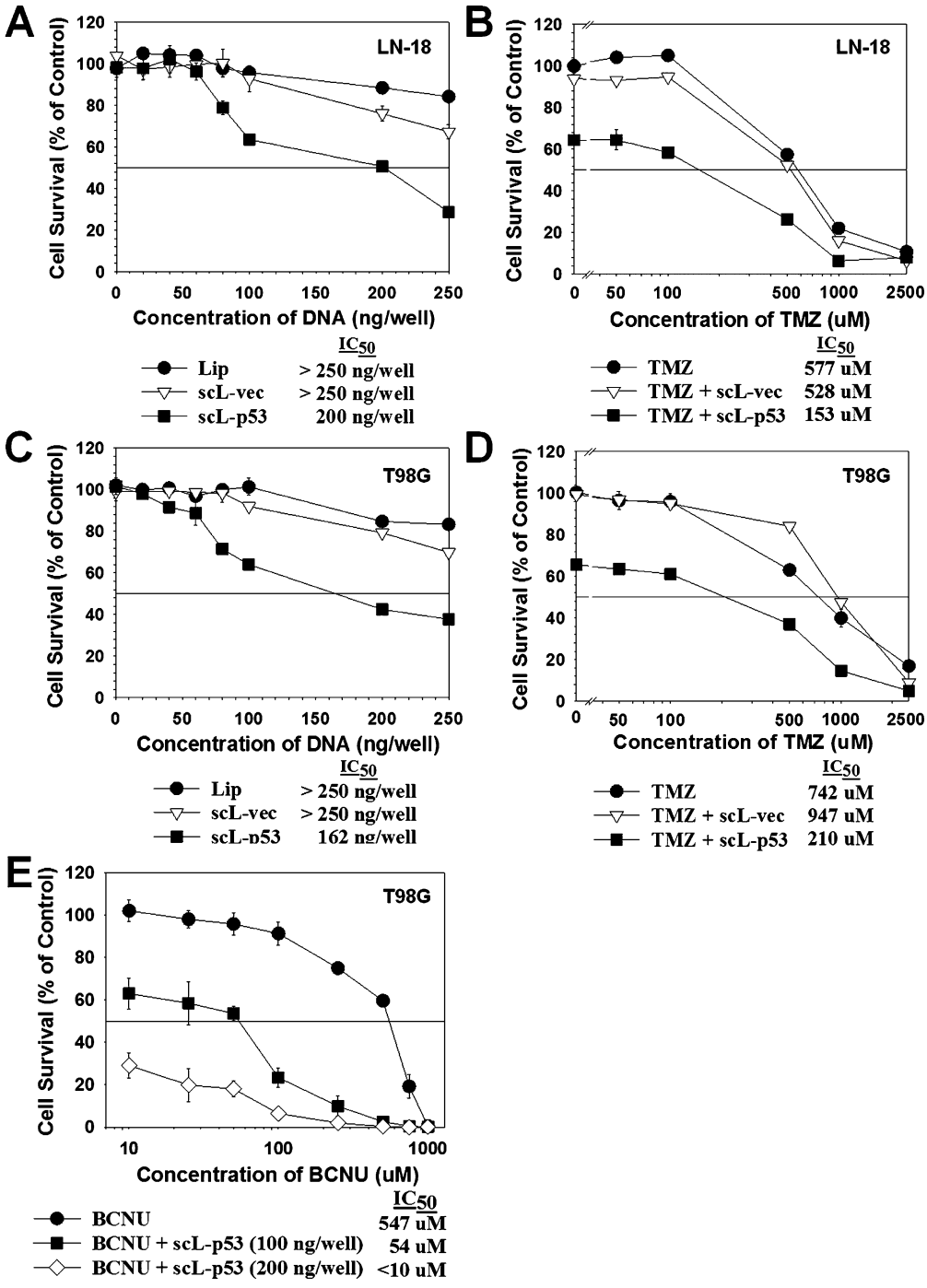

Figure 4. *In vitro* **sensitization of human GBM cell lines to TMZ and BCNU by scL-p53. TMZ-resistant human GBM cell lines, LN-18 (A) and T98G (C) were transfected with increasing concentrations of scL-p53. For comparison, cells were also treated with lipid alone (Lip) or scL-vec, the nanocomplex carrying the empty plasmid vector. 96 h later, cell viability was measured by XTT assay. For chemosensitization studies, LN-18 (B) and T98G (D) were transfected with scL-p53 (100 ng of DNA/well, which is equivalent to 50 pg of DNA/cell) for 24 h and then treated with increasing concentrations of TMZ for an additional 72 h. For comparison, cells were also treated with TMZ alone. (E) Comparison of cytotoxic effects of BCNU alone and BCNU in combination with scL-p53 in T98G cells. Cells were treated with increasing concentrations of BCNU for 72 h, either alone or 24 h after transfection with the scL-p53 nanocomplex (either 100 or 200 ng of DNA/well, which are equivalent to either 50 or 100 pg of DNA/cell, respectively).**

agents. As a result of treatment with scL-p53, the lack of MGMT to repair the DNA damage induced by chemotherapeutic agents such as TMZ, along with the exogenous wtp53's pro-apoptotic effect, could play a role in overcoming the resistance of T98G tumors to the killing effects of TMZ *in vivo*.

scL-p53-Mediated Potentiation of TMZ Effect and Increased Apoptosis in Highly TMZ-Resistant T98G Human Glioblastoma Cells *In Vitro*. To further study the scL-p53-mediated potentiation of TMZ-induced cell death in TMZ-resistant GBM, T98G cells were treated with TMZ at concentrations of 100 or 500 μM, either alone or in combination

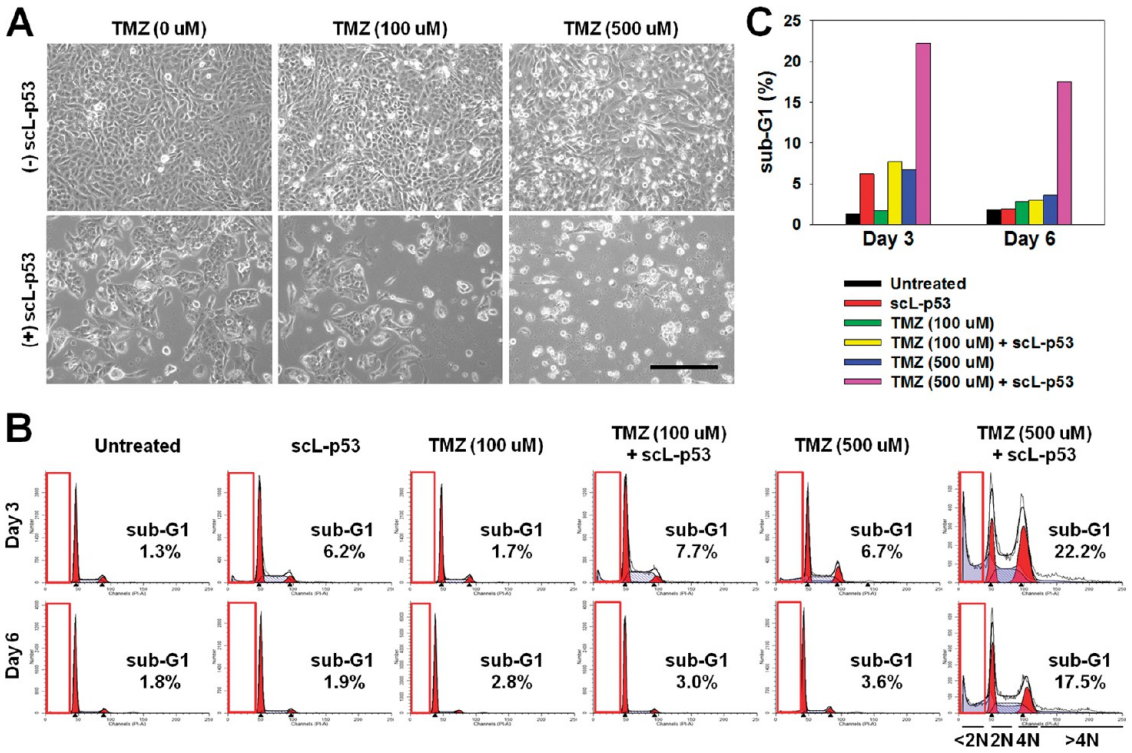

Figure 5. scL-p53-mediated enhancement of TMZ effect in highly TMZ-resistant human GBM cells. T98G cells were treated with the indicated concentrations of TMZ, either alone or after transfection with the scL-p53 nanocomplex (21 μg of DNA/dish, which is equivalent to 35 pg of DNA/cell) for 24 h. (A) Photomicrographs of representative area of the cell monolayer 3 days after TMZ treatment. Scale bar indicates 200 um. (B) Cell cycle profiles of T98G cells 3 and 6 days post-treatment with TMZ. The inset boxes indicate sub-G1 population. Numbers indicate the percentages of sub-G1 cells. (C) Quantification of the percent of cells in the sub-G1 population shown in B.

with scL-p53, and assessed for apoptosis. The cells were transfected with scL-p53 (21 μg of DNA/dish, which is equivalent to 35 pg of DNA/cell) 24 h prior to addition of TMZ. Three days later, the number of untreated T98G cells had increased to confluence without any evidence of cell detachment. In contrast, microscopic examination of cells treated only with TMZ and without scL-p53 revealed that there was at least some response to TMZ in a dose-dependent manner, with increasing numbers of detached, presumably dead, cells evident (Figure 5A). It was also evident that transfection with scL-p53 alone had sizable killing effect on T98G cells, greater than that observed with even the highest dose of single agent TMZ. However, the degree of apoptosis observed in the cells treated with the combination of scL-p53 and TMZ was significantly greater than with either single agent in a TMZ dose-dependent manner. These results indicate sensitization to the effects of TMZ leading to a major increase in TMZ-induced cell death in T98G cells as a result of treatment with scL-p53 nanocomplex.

The combination of TMZ and scL-p53 treatment also affected the cell cycle profile of T98G cells after TMZ treatment (Figure 5B). Although an increase in the G2 population was observed 3 days after TMZ treatment in all cells, this increase was significantly greater in the cells also transfected with scL-p53. This increase showed a TMZ-dose dependent response as well. Moreover, quantifying the percent of cells in the sub-G1 population, as an indicator of dead cells, showed that there was a time and TMZ dose-dependent apoptotic response (Figure 5C). The combination of scL-p53 and TMZ treatment significantly increased the sub-G1 population compared to TMZ treatment alone, especially with TMZ at concentration of 500 μM, demonstrating a scL-p53-mediated increase in response to the killing effects of TMZ of the previously resistant T98G cells.

Combination of TMZ and scL-p53 Nanocomplex Enhances Tumor Response and Induction of Apoptosis in Both CSCs and Bulk Tumor Cells in a T98G Subcutaneous Mouse Xenograft Model. The data presented above indicates that scL-p53 can down-modulate MGMT, which in turn results in sensitization of TMZ-resistant GBM cells to this first-line chemotherapeutic agent *in vitro*. To assess the clinical potential of this approach, we examined the T98G tumor response to TMZ after systemic administration of scL-p53 *in vivo*. Mice with subcutaneously established T98G xenografts were randomized and grouped for treatment with TMZ, either alone or in combination with systemically (i.v. tail vein) administered scL-p53 using the schedule shown in Figure 6A. Tumor response to treatment was assessed by measuring the tumor size (Figure 6B). While TMZ alone and scL-p53 alone had some inhibitory effect on tumor growth, the tumors in

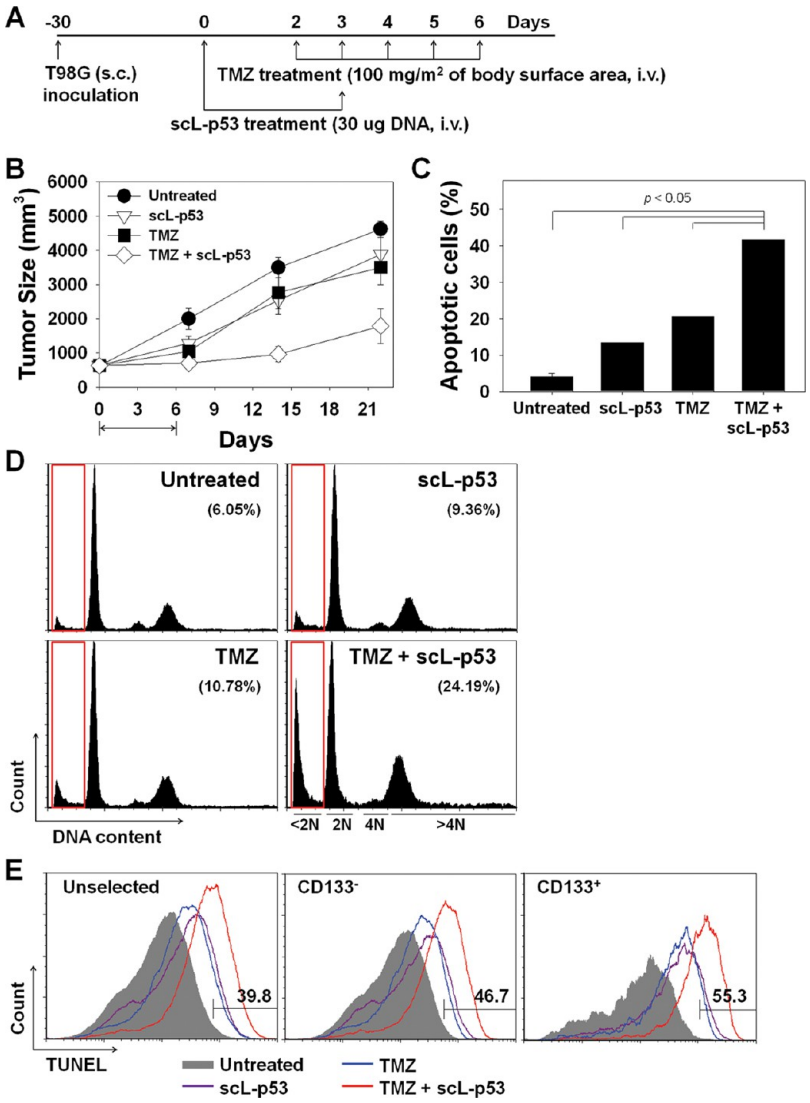

Figure 6. Enhanced tumor response and apoptosis in CSCs by the combination of TMZ and scL-p53 nanocomplex. Mice with subcutaneous T98G tumor xenografts were randomized to therapy with TMZ, either alone or in combination with scL-p53. Number of animals per treatment group = 4. (A) Treatment schedule. Mice received total 2 injections of scL-p53 and/or 5 injections of TMZ. (B) Comparison of tumor growth between different treatment groups. Arrow indicates the duration of the treatments. (C) Quantification of apoptotic cells in the tumor by Annexin V assay performed on day 9. The percentages of Annexin V positive cells in the tumors are shown. (D) Quantification of the apoptotic response represented by the percent of tumor cells in the sub-G1 population on day 9. The inset boxes indicate sub-G1 population. Numbers indicate the percentages of sub-G1 cells. (E) Quantification of apoptosis in the $CD133^+$ CSCs and $CD133^-$ bulk tumor cells by TUNEL assay performed on day 9. Numbers indicate the percentages of TUNEL positive cells in tumors treated with TMZ plus scL-p53.

both groups rapidly increased in size during treatment (respectively 1.5-fold and 1.9-fold increase on day 7 compared to tumor size at the start of treatment). In contrast, the tumors in the group of mice that received the combination of scL-p53 and TMZ displayed a significant tumor growth inhibition during the same period (1.1-fold increase). This significant inhibition of tumor growth continued after treatment ended on day 6, with only a 2.8-fold increase in tumor size by day 22, while TMZ alone and scL-p53 alone showed 5.5-fold and 6.1-fold increases, respectively.

To evaluate the antitumor response, the level of apoptosis induced in subcutaneous T98G tumors was determined by Annexin V (Figure 6C) and the cell cycle assay (Figure 6D) on day 9, which is 3 days after the completion of scL-p53 and/or TMZ treatment. There was a synergistic increase in the percent of the Annexin V positive tumor cells, indicative of apoptosis, after the combination of scL-p53 plus TMZ (~40%) compared to untreated control (~4%) or either treatment alone (~14 and ~20% for scL-p53 and TMZ respectively) (Figure 6C). Similarly, there was a significant increase in the percent of cells in sub-G1 in the cell cycle, confirming increased apoptosis after the combination treatment. The percent of cells in sub-G1 in the tumor treated with both scL-p53 and TMZ was ~ 24% compared to those in the untreated tumors (~6%) or treated with single agent (~9 and ~10% for scL-p53

and TMZ respectively) (Figure 6D). Thus, these results indicate that uptake of systemically administered scL-p53 by the tumors results in an enhanced apoptotic response to chemotherapeutic agent TMZ.

Importantly, scL-p53 treatment also sensitized $CD133^+$ CSCs to TMZ treatment in these subcutaneous T98G tumor xenografts (Figure 6E). Quantification of apoptosis by terminal deoxynucleotidyl transferase dUTP nick-end labeling (TUNEL) assay double labeled with CSC marker CD133 demonstrated increased apoptosis in both $CD133^+$ CSCs (~55%) and $CD133^-$ tumor cells (~47%) subpopulations when treated with combination of scL-p53 plus TMZ. In contrast, in the mice treated with scL-p53 alone the percent of apoptotic cells was only ~14% for both $CD133^+$ and $CD133^-$, while in those treated with TMZ alone it was just ~9% for both $CD133^+$ and $CD133^-$ cells. Therefore, the demonstration of this increased response to chemotherapeutic agent TMZ in CSCs after systemic treatment with scL-p53 shows that this combination approach may also be able to decrease the potential for development of drug resistance and recurrence in these tumors.

Enhanced Tumor Response to the Combination Treatment in an Intracranial Orthotopic Xenograft Mouse Model of Glioblastoma. As the above experiments demonstrated significant tumor response with the combination of scL-p53 and TMZ in a subcutaneous T98G xenograft model, we wanted to assess the effect of this combination therapy on tumor growth in a model more representative of the clinical situation. Thus, we established intracranial orthotopic T98G xenografts in mice. Upon the basis of the tumor size determined by MRI, prior to treatment the mice were grouped (7−11 mice per group) to yield approximately equal average tumor sizes in each group. The animals were treated with TMZ, either alone or in combination with systemically administered scL-p53 (i.v. *via* tail vein). Two doses of TMZ were employed in this study: a low dose of 100 mg/m^2 of mouse body surface area for 21 consecutive days and a high dose of 200 mg/m^2 of body surface area for 5 consecutive days (Figure 7A). Both of these TMZ regimens mimicked a single treatment cycle being used in the clinic.

As observed in the subcutaneous tumor study above, a significant inhibition of tumor growth was evident on both treatment schedules with the combination treatment of scL-p53 and TMZ as monitored by MRI (Figure 7B). In these studies tumor measurements by MRI ceased at day 22. At day 22 all of the mice treated with scL-p53 alone succumbed to their disease. Of the animals treated with TMZ alone at 200 or 100 mg/m^2, the majority succumbed to disease within 2−3 days; only 16.6 and 33%, respectively, of these animals were surviving. It should also be noted that all of the untreated mice had succumbed to their disease prior to day 22. While TMZ alone and scL-p53 alone had some inhibitory effect on tumor growth, the tumors in the group of mice that received the combination of scL-p53 and TMZ displayed significantly stronger response with both treatment regimens (Figure 7C). In the mice that received the combination treatment, the greatest degree of tumor inhibition was observed using the 21 day continuous treatment with the lower (100 mg/m^2) dose of TMZ.

However, even using the high dose regiment of 200 mg/m^2 TMZ for 5 days, significant inhibition of tumor growth was also evident, particularly at day 10, which was 5 days after the end of TMZ treatment. Although tumor volumes increased by day 22, tumors treated with this combination scL-p53/TMZ regimen were still significantly smaller compared to treatment with either single agent. Thus, in this highly TMZ-resistant brain tumor model, the combination of scL-p53 and TMZ (using multiple dosing regimens) results in a significant increase in tumor growth inhibition.

Increased Survival of Mice Bearing TMZ-Resistant Intracranial GBM Tumors after Treatment with the Combination of scL-p53 and TMZ. The above *in vivo* study demonstrated that treatment with scL-p53 was able to sensitize intracranial tumors derived from TMZ-resistant T98G cells to this chemotherapeutic agent when TMZ was administered at a dose of 100 mg/m^2 for 21 consecutive days. Therefore, a second experiment was performed to assess the survival benefit derived from this combination treatment regimen in mice bearing intracranial tumors derived from TMZ-resistant T98G cells. This schedule of daily TMZ administration for 21 consecutive days is similar to one that has been employed in various clinical trials with human patients.

Since only small amounts of tumor remain post-surgical resection of intracranial tumors in GBM patients, compared to the experiment described above (Figure 7), in this study we used a lower number of these highly aggressive T98G cells to establish the intracranial tumors in the mice in an attempt to be somewhat more representative of the clinical situation. As shown in the schematic of the treatment schedule (Figure 8A), TMZ was administered daily from days 1 through 21. scL-p53 was administered 1 day before the initiation of TMZ treatment and thereafter twice weekly to day 31 for a total of 10 injections. As controls, groups of mice also received scL-p53 only, TMZ only, or remained untreated (11−15 mice per group).

In order to assess the increased response of previously resistant GBM intracranial tumors to TMZ by treatment with scL-p53, the difference in survival between TMZ alone and in combination with scL-p53 was evaluated (Figure 8B).

In the *in vivo* efficacy study shown in Figure 8A,B, the animals received only one cycle of treatment, which ended by day 31. Compared to the untreated mice, there was a minimal increase in survival after treatment with scL-p53 alone. Typically, 100% of the mice receiving TMZ only succumb to disease around day 43. However, in this particular experiment 13% of

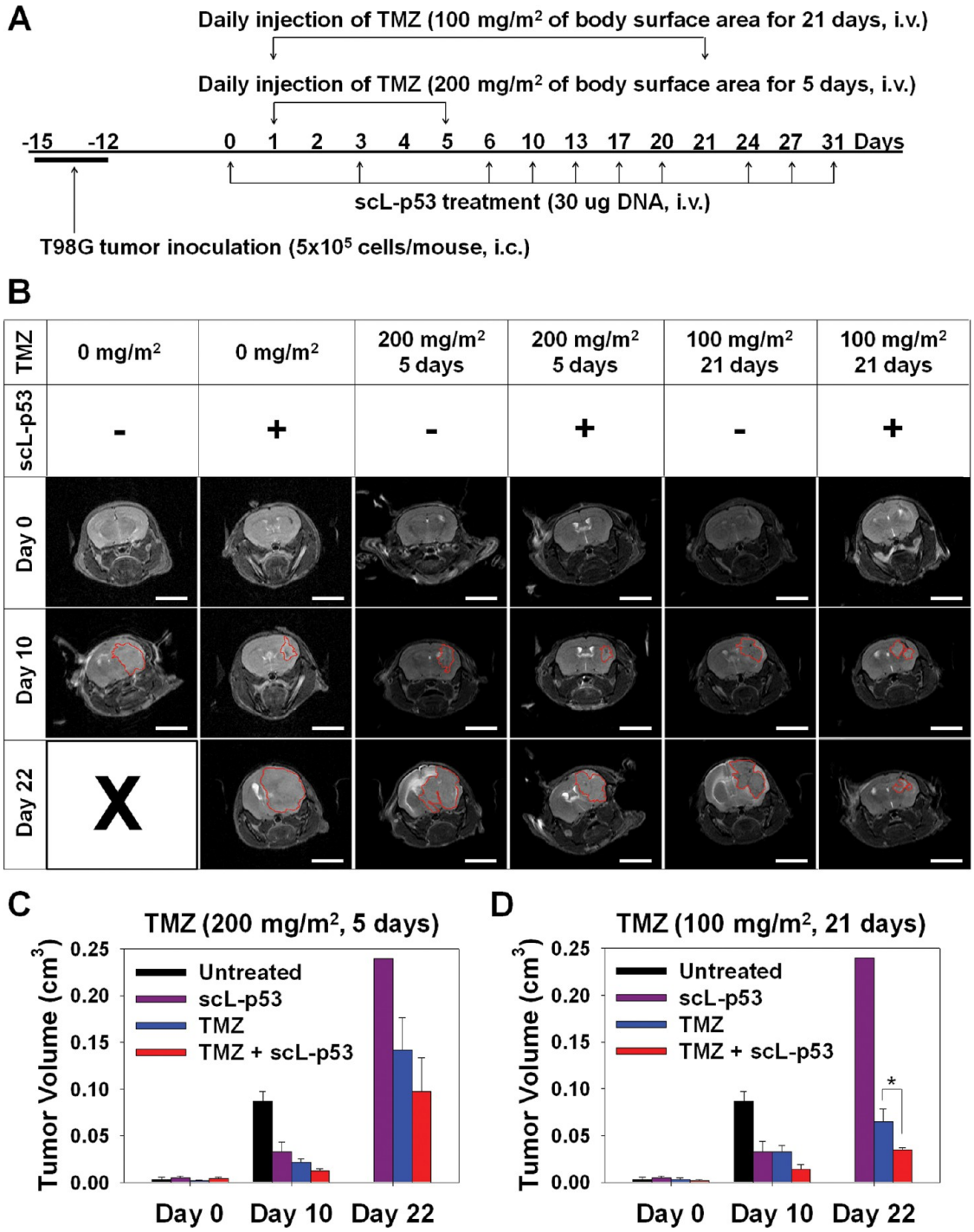

Figure 7. Enhanced tumor response by the combination of TMZ and scL-p53 nanocomplex in an orthotopic GBM model. Mice with intracranially established T98G xenograft tumors were randomized to groups and treated with TMZ in combination with scL-p53, or with either agent alone. (A) Treatment schedule. Mice received total 10 injections of scL-p53 and/or either 5 or 21 injections of TMZ. (B) MR imaging of intracranial T98G tumors. MR image was collected before the initiation of treatment (day 0) and during treatment (day 10 and day 22). Red lines indicate the outline of the brain tumors. Scale bar = 0.5 cm. Quantification of tumor volume from MRI measurement: (C) mice treated with 200 mg/m^2 of body surface area of TMZ (5 days) or (D) mice treated with 100 mg/m^2 of body surface area of TMZ (21 days). Number of animals per treatment group = 7–11. *$P < 0.05$.

the mice survived to day 51. In contrast, 46% of the mice that received the combination of scL-p53 and TMZ were surviving at day 51. A log rank statistical analysis for the survival curves was performed. The log rank statistic is greater than would be expected by chance; thus, there is a statistically significant difference between survival curves ($P < 0.001$). Although the mice receiving the combination treatment succumbed to disease by day 56, these results demonstrate that 20 days after the end of treatment (day 51), there was a

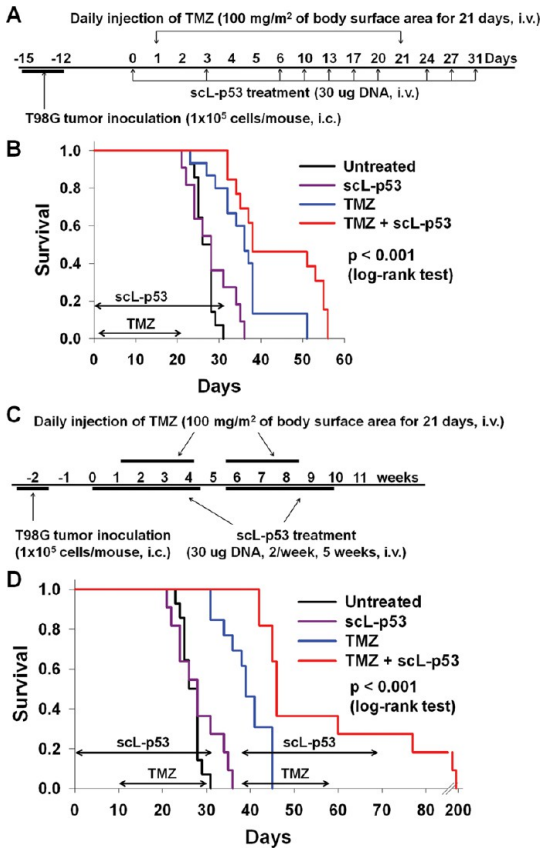

Figure 8. Increased survival by combination of TMZ and scL-p53 nanocomplex in an orthotopic GBM model. Mice with intracranially established T98G xenograft tumors were randomized to groups and treated with TMZ in combination with scL-p53, or with either agent alone. (A) Single cycle treatment schedule. Mice received total 10 injections of scL-p53 and/or 21 injections of TMZ. (B) Kaplan–Meier survival curves. Number of animals per treatment group = 11–15. (C) Two cycle treatment schedule. Mice received 10 injections of scL-p53 and/or 21 injections of TMZ in each cycle. (D) Kaplan–Meier survival curves. Number of animals per treatment group = 11–15.

significant difference in survival when scL-p53 is administered in combination with TMZ, compared to TMZ alone.

In the clinic, TMZ is administered in multiple cycles. While the data in Figure 8B supports the hypothesis that scL-53 sensitizes these TMZ resistant cells to chemotherapy after a single cycle of treatment, we wished to determine if an additional cycle could enhance survival benefit in TMZ resistant T98G tumors. Thus, tumors were again induced by intracranial injection of T98G cells using the identical number of cells as in Figure 8A,B. Two cycles of treatment with either TMZ alone or the combination of scL-p53 plus TMZ was administered as shown in the schematic in Figure 8C (11–15 mice/group). As shown in Figure 8D, a second cycle of TMZ alone had minimal increase on survival. These mice all succumbed to disease by day 45. In contrast, 63.6% of the mice were still alive at day 45 when scL-p53 was added to TMZ. Moreover, 36% of these mice survived to 60 days, 27% survived to 77 days, 18% survived to 137 days and 9% of the mice survived to 177 days. Here also the log-rank analysis demonstrated a statistically significant difference between the survival curves, specifically, there was a statistically significant difference ($p = 0.00203$) between the TMZ only and the scL-p53 plus TMZ groups.

These findings, along with the fact that the scL-p53 alone resulted in no major change in survival time, indicates the synergistic effect of this combination regimen, in mice bearing TMZ-resistant intracranial tumors. They also demonstrate that multiple cycles of the combination of scL-p53 and TMZ (administered at 100 mg/m^2 daily for 21 days) can increase survival in mice bearing TMZ-resistant intracranial tumors.

DISCUSSION

Although the current standard of care for GBM has shown a significant improvement, the overall survival benefit is only moderate. This is likely, in part, due to the inherent TMZ resistance of GBM tumors (in 60–75% of patients) and frequent tumor recurrence. Studies have indicated that MGMT-mediated DNA repair is the clinically relevant primary mechanism of resistance to TMZ.[42,43] Thus, inhibition of MGMT activity, or a decrease in MGMT protein levels, should result in an increase in response to this chemotherapeutic agent. While the contribution of MGMT to TMZ-resistance is heavily documented, there are also tumors in which MGMT is not the primary determinant of treatment resistance but which involve several independent DNA repair systems (*i.e.*, base excision repair, strand break repair, *etc.*).[44–46] However, in the present study, we have focused on MGMT-conferred resistance to TMZ.

The role of p53 in the response to TMZ has been addressed in a number of preclinical studies in which conflicting results can be found.[44] Published reports have suggested either an increase[47–50] or a decrease[51–53] in TMZ efficacy through transient inhibition of wtp53 function either by oncoprotein E6, small molecule inhibitor pifithrin-α, or anti-p53 siRNAs. However, there are other reports that clearly support the role of wtp53 in response to TMZ. Stable knockdown of p53 using shRNA strongly attenuated TMZ cytotoxicity indicating that p53 is required for TMZ-induced apoptosis.[53] Furthermore, agents designed to stabilize the wild-type conformation of p53 sensitized glioblastoma cells to TMZ.[51,54] Therefore, as wtp53 does seem to play an important role in resistance to TMZ; here we assessed the ability of the wtp53 gene, when delivered *via* the scL nanocomplex, to overcome TMZ resistance in GBM tumors *in vitro* and *in vivo*.

In the above experiments we demonstrated that, taking advantage of elevated levels of the TfR on the brain endothelium, the systemically administered scL-p53 nanocomplex is able to cross the BBB and efficiently deliver its payload to intracranial tumors. This efficient delivery of wtp53 resulted in a virtually complete down-modulation of MGMT expression in these

T98G derived tumors. Although the molecular link between p53 and MGMT has not been extensively studied to date, the p53-mediated sequestration of specificity protein 1 (Sp1), a transcription factor that binds to the MGMT promoter, could be one of the mechanisms by which p53 negatively regulates MGMT expression.[8]

p53-induced abrogation of MGMT expression would limit the ability of GBM cells to remove the O^6-methylguanine DNA adducts, thus resulting in cell cycle arrest and apoptosis. Consistent with this hypothesis, treatment of MGMT-proficient and highly TMZ-resistant T98G and LN-18 cells with scL-p53 was able to significantly increase the response of these cells to TMZ *in vitro*.

More importantly, similar results consistent with this hypothesis were observed *in vivo*. In mice bearing subcutaneous T98G tumors, the combination of systemically administered scL-p53 and TMZ led to substantial inhibition of tumor growth and increased apoptosis. Of even more significance with respect to the clinical potential of this approach, the ability of scL-p53 to cross the BBB and target intracranial tumors led to the sensitization of these previously resistant tumors to TMZ resulting in increased survival. These findings suggest that patients may be more likely to respond to the combination of scL-p53 and TMZ than TMZ therapy alone. In addition, the survival benefit observed with multiple cycles of the combination treatment could be further enhanced by adding fractionated radiation since concurrent radiation and TMZ is the standard treatment regimen and scL-p53 has been shown to increase the response of tumors to radiation in mice.[22] The effect of this triple combination has yet to be explored.

The poor overall survival of GBM patients is due in part to tumor recurrence. Compounding the problem, these recurrent GBM tumors are often more resistant to conventional treatments, such as TMZ, to which they initially responded. CSCs, a small population of cells possessing stem cell-like properties, are thought to be responsible for therapeutic resistance, cancer recurrences, and metastasis in various types of cancer including GBM.[54−56] Drug treatment of malignant GBM is limited by the intrinsic resistance of GBM CSCs to chemotherapy.[57,58] Thus, therapeutic strategies directed at eliminating CSCs would be a rational approach to improve anticancer efficacy. In our previous studies, we have demonstrated the ability of scL to target both CSCs and differentiated bulk tumor cells in GBM xenografts using multiple markers of CSCs including CD133, SSEA-1, Nestin, Nanog, and Msi1.[32] In the present study, we demonstrated *in vivo* that systemically administered scL crossed the BBB, targeted and efficiently delivered a fluorescently labeled ODN payload to both CSCs and bulk tumor cells in intracranial tumors. Of note, these studies also demonstrated the release of the payload from endosomes (an intracellular membrane-bound compartment that mediates the transport of receptor-bound signaling complexes into the cell),[59] into the cytoplasm and ultimately nucleus in both populations. These results mirror our previous observations *in vitro*.[32] In a time course study of the uptake of scL-6FAM-ODN in tumor cells, we also observed the same sequence of intracellular trafficking of the 6FAM-ODN from entry through receptor-mediated endocytosis, release from the endosomes with diffuse fluorescence signal throughout the cytoplasm, and ultimately the strong presence of the fluorescence signal in the nucleus. This previously published[32] time course is presented in the Supporting Information as Figure S4.

Furthermore, scL-p53 treatment in combination with TMZ resulted in extensive apoptosis of $CD133^+$ CSCs in intracranial GBM tumor xenografts. In line with our data, in a recent study on the effect of p53 status on the response of GBM CSCs to TMZ, it was demonstrated that CSCs are resistant to TMZ when p53 is mutated and sensitive to TMZ when p53 is intact.[50] Although the role of p53 in CSCs of GBM has not been completely delineated, in addition to MGMT down-modulation shown here, it has been suggested that p53 controls the differentiation, self-renewal and tumorigenic potential of GBM CSCs by negatively regulating the GLI1-NANOG network.[14,60] It was also shown that disruption of p53, together with inactivation of PTEN, enhanced self-renewal and impeded differentiation capacity of neural stem cells and GBM CSCs by elevating c-Myc activity.[61] Thus, as a potential therapeutic, scL targeted delivery of wtp53 to CSCs in GBM as shown here can result in the dual benefit of both MGMT down-modulation to increase response of CSCs to TMZ and decreased self-renewal/increased differentiation of CSCs in GBM. Together these should reduce both the development of resistance to standard therapy and tumor recurrence.

Although TMZ is relatively well tolerated, there are dose-dependent side effects including severe myelosuppression, which limit therapeutic dosages.[62] Extended use of TMZ treatment also provokes lymphocytopenia and increases opportunistic infections.[63] In this regard, an additional advantage of scL-p53-mediated sensitization of GBM tumors to TMZ is the potential to lower the effective therapeutic dose of the chemotherapeutic agent. In addition to increasing patients' quality of life, reducing the side effects is crucial as the patients often receive multiple cycles of TMZ treatment, which can be interrupted or discontinued on the basis of the severity of the side effects.

CONCLUSION

The results presented here suggest that combining scL-p53, which in clinical trials has so far shown to have minimal side effects and to have anticancer effects,

with standard TMZ treatment could be a more effective therapy for GBM. Moreover, TMZ is also being evaluated in clinical trials for treatment of other types of cancer including melanoma,[64,65] pancreatic cancer,[66] neuroendocrine cancer,[67] and brain metastases from non-CNS solid tumors such as nonsmall cell lung cancer and breast cancer.[68] Thus, the potential of the combination of scL-p53 and TMZ to enhance treatment efficacy is likely not limited to GBM. Furthermore, MGMT-dependent resistance to other alkylating agents, such as BCNU, CCNU, and 6-thioguanine, has also been observed with MGMT overexpression in, *e.g.*, melanoma, pancreatic, lung, and neuroendocrine cancers.[16,69−72] Here, we also observed p53 sensitization to BCNU induced cell death suggesting that scL-p53 can likely sensitize tumors to other alkylating agents. Thus, this approach has the potential for broad clinical application.

MATERIALS AND METHODS

Drugs. TMZ (Sigma, St. Louis, MO) was dissolved in DMSO (Sigma) at a stock concentration of 100 mM. BCNU (Carmustine, Bristol-Myers Squibb, Evansville, IN) was dissolved in ethanol (Sigma) to a concentration of 100 mM.

Cell Lines. Human GBM cell lines U87, T98G, and LN-18 were obtained from American Type Culture Collection (Manassas, VA). U87 has wtp53, while the T98G and LN-18 cell lines carry mt p53.[73,74] Cells were maintained at 37 °C in a 5% CO_2 atmosphere in modified IMEM (Gibco, Grand Island, NY; U87), MEM (Mediatech, Manassas, VA; T98G) or DMEM (Mediatech; LN-18) supplemented with 10% heat-inactivated fetal bovine serum (FBS, Omega Scientific, Tarzana, CA), 2 mM L-glutamine (Mediatech), and 50 μg/mL each of penicillin, streptomycin, and neomycin (Gibco).

Preparation of scL-p53 Nanocomplex. Cationic liposome 1,2-dioleoyl-3-trimethylammonium propane (DOTAP)/dioleolylphosphatidyl ethanolamine (DOPE) (Avanti Polar Lipids, Alabaster, AL), referred to as Lip, was prepared as described previously.[23] TfRscFv/Lip/p53 (scL-p53, scL encapsulating plasmid DNA encoding wt human p53) complex and scL-ODN (scL encapsulated oligonucleotide) complex were prepared as previously described.[24] For *in vitro* experiments, the complex was further diluted with serum-free medium. The size and zeta potential of the complex was determined by DLS at 25 °C with a Zetasizer Nano ZS System (Malvern Instruments, Malvern, UK).

Atomic Force Microscopy. AFM was performed at the National Institute of Standards and Technology (NIST) essentially as previously described.[33,34] Cationic liposomes and nanocomplexes are adsorbed either on freshly cleaved mica or on UV/ozone treated poly-L-lysine coated mica (PLL-mica). The latter is prepared by immersing a freshly cleaved mica disk in a 0.01% PLL solution for 30 min and, after blow drying, exposing it to UV/ozone to tune the surface zeta potential of the freshly prepared PLL-mica. During the 0−30 min exposure, the PLL-mica substrate is placed 1 cm apart from a UVP-51 lamp (UV Products) in a sealed metal box located in a fume hood in ambient air.

For fluid AFM imaging, samples were diluted using deionized water (1:10), and a 5 μL droplet of the liposome/complex solution was deposited onto freshly cleaved mica or PLL-mica and incubated for 1 min. The sample was immersed in water to remove unattached liposomes and imaged in 5 mM $MgCl_2$ imaging buffer. For dry SPM imaging, 5 μL droplet of the liposome solution was deposited onto freshly cleaved mica, incubated for 1 min and washed with PBS. AFM imaging was performed with a Veeco MultiMode AFM and Nanoscope IV controller. Nanoscope Version 6 software was used for data acquisition. Dry imaging was performed in TappingMode using Veeco OTESP cantilevers. For fluid imaging, a TappingMode fluid cell, without an O-ring, and Veeco OTR8 'B' cantilevers (24 kHz nominal resonance frequency in air) were used by oscillating the cantilever in the low-frequency acoustic mode region, *ca.* 7−9 kHz. SPM calibration was performed using a series of negatively charged, citrate-stabilized gold nanoparticles with nominal sizes of 10, 30, 50, and 80 nm (Ted Pella, Inc., Redding CA). Particle-size analysis using SPM image data was performed using resources available in Nanoscope Version 5 and ImageJ. DLS and ZP measurements were performed using a Zetasizer Nano ZS system. Each sample was diluted with deionized water, loaded into a disposable microcuvette and measured at 25 °C. Size distributions were calculated using the "general purpose" non-negatively constrained least-squares method.

Assessing Efficiency of DNA Encapsulation. To monitor the encapsulation (loading) efficiency of plasmid DNA in the scL nanocomplex, the mobility of free DNA was assessed by agarose gel electrophoresis. Electrophoresis in a 0.6% agarose gel (TBE buffer containing 0.2 mg/mL ethidium bromide) was performed using various amounts of plasmid DNA encoding wt human p53 either encapsulated in the scL nanocomplex or as free plasmid DNA. The gel was run at 90 V for approximately 2 h, and the DNA was visualized and photographed by UV light.

XTT Assays. Cell viability was measured by sodium 3′-[1-(phenylamino-carbonyl)-3, 4-tetrazolium]-bis(4-methoxy-6-nitro)-benzenesulfonate (XTT) assay (Polysciences, Warrington, PA). T98G and LN-18 cells (2.0×10^3 cells/well in 96-well plates in triplicates) were treated with either the scL-p53 or the scL-vec nanocomplexes at increasing concentrations (0−250 ng of DNA/well). 96 h post-treatment, cell viability was determined by the XTT assay, and the IC_{50} values, the drug concentration resulting in 50% cell death, were interpolated from the graph of the log of DNA concentration *versus* the fraction of surviving cells using SigmaPlot (Systat Software Inc., San Jose, CA).

To assess the degree of sensitization to TMZ, T98G and LN-18 cells (2.0×10^3 cells/well in 96-well plates in triplicates) were treated with the either the scL-p53 or scL-vec nanocomplexes (100 ng of DNA/well) for 24 h, followed by the addition of increasing concentrations of TMZ (0−2500 μM). 72 h after the addition of TMZ (and 96 h after scL-p53 treatment), cell viability was determined by the XTT assay and the IC_{50} values were calculated as above.

In another experiment, T98G cells (2.0×10^3 cells/well in 96-well plates in triplicates) were treated with the scL-p53 nanocomplex (either 100 or 200 ng of DNA/well) for 24 h, followed by the addition of increasing concentrations of BCNU (10−1000 μM). 72 h after the addition of BCNU, cell viability was determined by the XTT assay and the IC_{50} values were calculated as above.

***In Vitro* Sensitization Study.** TMZ sensitization was evaluated by assessing the presence and level of apoptosis in cancer cells as determined by the percent of cells in the sub-G1 population of the cell cycle. T98G cells (6.0×10^5 cells/dish in 10 cm cell culture dishes) were treated with scL-p53 nanocomplex (21 μg of DNA/dish) for 24 h, after which the cells were treated with different amounts of TMZ. 72 h after the addition of TMZ, the cells and supernatant media were collected, and the amount of apoptosis was assessed. Collected cells were fixed in cold ethanol (70% vol/vol) and stained with PI (BD Pharmingen, San Diego, CA). DNA content was measured by BD FACS Aria flow cytometer (BD Biosciences, San Diego, CA), and histograms were analyzed by DNA ModFit LT software (Verity Software House, Topsham, ME).

Animal Model. All animal experiments were performed in accordance with and under approved Georgetown University GUACUC protocols. For the subcutaneous GBM tumor model, 5−6 week old female athymic nude mice (Harlan Sprague−Dawley, Indianapolis, IN) were inoculated with T98G cells (5.0×10^6 cells per site) suspended in Matrigel (BD Bioscience,

Inc.) on the lower back, above the tail.[75] For the orthotopic intracranial GBM tumor model, 5−6 week old female athymic nude mice were stereotactically inoculated with either U87 or T98G cells. For injection, trypsinized U87 or T98G cells were resuspended in cold phosphate-buffered saline at 1.0×10^5 cells/μL. A total of either 5.0×10^5 cells in 5 μL volume or 1.0×10^5 cells in 1 μL volume were injected into the right hemisphere of the mouse brain (0.5 mm posterior to the bregma, 2.5 mm lateral to the midline, and 3.5 mm depth from skull) at a speed of 1.0 μL/min using a 10 μL sterile Hamilton syringe fitted with a 26-gauge needle attached to a stereotaxic frame (Stoelting, Wood Dale, IL). Wounds were closed with sterile wound clips and animals were carefully monitored until recovered from anesthesia.

***In Vivo* Tumor Targeting Study.** Three weeks after inoculation of intracranial U87 tumor cells, mice received a single i.v. injection with 25 μg of Cy5-ODN complexed with scL (scL-Cy5-ODN), Lip (Lip-Cy5-ODN), or as free Cy5-ODN (25 μg). At 24 h after the injection, tumor-bearing brain was imaged with the Maestro *in vivo* fluorescence imaging system (CRi Inc., Woburn, MA). The resulting acquisition images were analyzed, and the fluorescence signal intensity was quantified using the vendor's software (Maestro 2.10.0). Signal intensity is expressed as photons/cm^2/second. After imaging, single-cell suspensions were obtained from the tumors by collagenase digestion.[32] To identify the CSC population, single cells were stained with antibodies against human CD133-PE (Miltenyi Biotec, Auburn, CA) and human SSEA-1 (Stemgent, San Diego, CA). The labeled cells were analyzed by BD FACS Aria flow cytometer.

In another study, mice with established intracranial U87 tumors were injected with scL-6FAM-ODN (100 μg of 6FAM-ODN/mouse/injection). At 24 h postinjection the mice were sacrificed, and brains were snap-frozen. Cryosections (10 μm) were prepared and stained with rabbit polyclonal anti-CD133 antibodies (Abcam, Cambridge, MA) followed by Texas Red-conjugated secondary sheep antirabbit IgG antibodies (Abcam) according to the manufacturer's protocol for staining of frozen sections. After incubation, slides were mounted with ProLong antifade kit (Molecular Probes, Eugene, OR) and observed with an Olympus Fluoview-FV300 Laser Scanning Confocal System (Olympus, Center Valley, PA).

To assess tumor specificity in the brain, mice with established intracranial T98G tumors were injected with scL-Cy5-ODN (25 μg of Cy5-ODN/mouse/injection). At 24 h postinjection the mice were humanely euthanized, and tumor-bearing brains were harvested. After dissecting the brain tumors from the normal brains, single-cell suspensions were obtained from the tumors as described above. Normal brain cells were also isolated by mechanical dissociation (trituration), and the cell suspension was passed through a 70-μm cell strainer. To identify the CSC population, tumor cells were stained with antibodies against human CD133-PE and human SSEA-1. To identify the major normal brain cell types, the normal brain cells were stained with mouse CD11b-PE-Cy7 antibodies (BD Pharmingen) or primary antibodies against MAP2 (Abcam), GFAP (Abcam), nestin (Sigma) and MBP (Abcam) and detected with DyLight 488-conjugated secondary antibodies (BioLegend, San Diego, CA). The labeled cells were analyzed for uptake of Cy5-ODN by BD FACS Aria flow cytometer.

Western Blot Analysis. To determine the protein expression level, Western blot analysis was performed. For the *in vitro* study, T98G cells (6.0×10^5 cells/dish in 10 cm cell culture dishes) were transfected with either the scL-p53 or scL-vec nanocomplex (7 μg of DNA/dish). Sixteen and 24 h post-transfection, the cells were collected for western analysis. For the *in vivo* study, two models of T98G tumor xenografts (subcutaneous and intracranial) were used. Mice with established T98G tumor xenografts received either a single systemic injection (intracranial) or 3 injections over a 24 h period (subcutaneous) (i.v. *via* the tail vein) of scL-p53 (30 μg of wtp53 plasmid DNA per injection per mouse). At the indicated times after the treatment, the mice were humanely euthanized, and tumors were harvested. Protein was isolated, and 40 μg of total cellular protein was separated on an 8% SDS-polyacrylamide gel, transferred to nylon membrane, and hybridized with antibodies against human MGMT (Cell Signaling Technology, Beverly, MA), p53 (Calbiochem, San Diego, CA), p21 (Calbiochem), and cleaved PARP (Cell Signaling Technology). An antibody recognizing glyceraldehyde-3-phosphate dehydrogenase (GAPDH) (Trevigen, Gaithersburg, MD) was utilized as an internal control for protein loading. Chemiluminescent detection was carried out using an ECL kit (GE Healthcare Life Sciences, Pittsburgh, PA). Quantification of protein band was carried out using ImageJ software (http://rsb.info.nih.gov/ij/).

***In Vivo* Response and Survival Studies.** The *in vivo* response to the combination of scL-p53 and TMZ was assessed by determining the level of apoptosis in the tumors using Annexin V, cell cycle, and TUNEL assays. Mice with subcutaneously established T98G tumor xenografts received systemic injection (i.v. *via* the tail vein) with either 30 μg (per injection per mouse) of wtp53 plasmid DNA encapsulated in scL (scL-p53), or with 100 mg/m^2 (per injection per mouse) of TMZ, or the combination of both following the indicated treatment schedules given in Figure 6A. On day 9, 3 days after the last TMZ treatment, tumors were harvested, weighed, and cells were dissociated by enzymatic digestion as above. Cells were passed through a 70 μm cell strainer (Fisher Scientific) and subjected to Annexin V staining. For TUNEL assay, isolated cancer cells were double labeled with a CSC marker, human CD133-PE (Miltenyi Biotec) and *in situ* cell death detection kit (Roche Applied Science), and analyzed by flow cytometry.

Mice with intracranially established T98G tumor xenografts were systemically i.v. tail vein injected with either 30 μg (per injection per mouse) of scL-p53, or with 100−200 mg/m^2 (per injection per mouse) of TMZ, or the combination of both following the indicated treatment schedules given in Figure 7A and Figure 8A. All mice were euthanized when they became moribund. Survival was monitored and plotted using the Kaplan−Meier method. Log-rank test was used to test the significance of different survival curves (SigmaPlot).

Magnetic Resonance Imaging. To visualize and measure the intracranial tumors, animals were imaged *in vivo* without the aid of a contrast agent on a 7 T Bruker horizontal spectrometer/imager run by Paravision 5.1 software (Bruker Biospin MRI GmbH, Karlsruhe, Germany). Animals were maintained under anesthesia with 1.5% isoflurane and 30% nitrous oxide and placed in a custom-designed stereotaxic animal holder outfitted with temperature and respiration monitoring capacity. A four-channel receive-array mouse brain coil and a transmit volume coil were used to run a two-dimensional T2-weighted TURBO-RARE protocol with the following parameters: TR, 4660 ms; TE, 36 ms; Matrix, 256×256; FOV, 3.5×3.5 cm; Slice thickness, 0.5 mm; and Averages, 4.

Bruker Paravision 5.1 software was used to calculate tumor volumes. The regions of interest (ROIs) containing tumor were determined on the basis of the contrast differential exhibited by brain tumors *versus* normal brain and manually traced. Volumes were determined by multiplying area times slice thickness.

Statistical Analysis. The statistical significance was determined by Student's *t* test and by one-way analysis of variance (ANOVA). *P*-values of <0.05 were considered significant. Statistical significance for Kaplan−Meier curves was determined by log rank analysis. All graphs and statistical analysis were prepared using SigmaPlot.

Conflict of Interest: The authors declare the following competing financial interest(s): Drs. Chang and Pirollo are two of the inventors of the described technology, for which several patents owned by Georgetown University have been issued. The patents have been licensed to SynerGene Therapeutics Inc. for commercial development. Dr. Chang owns equity interests in SynerGene Therapeutics Inc. and serves as a non-paid scientific consultant to SynerGene Therapeutics Inc.

Acknowledgment. We thank K. Creswell and M. Chen, Flow Cytometry Shared Resource, Georgetown University Medical Center, for their technical assistance with flow cytometry. We also thank M. Burns, Department of Neuroscience, Georgetown University, for his helpful technical consultation with executing the stereotactic inoculation. We also thank O.C. Rodriguez and Y.C. Lee, Preclinical Imaging Research Laboratory, Georgetown University Medical Center, for their assistance with MRI imaging

and analysis and B. Kallukry for his help in evaluating the tissue sections. This study was supported in part by NCI Grant 5R01CA132012-02 (E.H.C.) and a research grant from SynerGene Therapeutics Inc. (K.F.P.). This study was conducted in part using the Flow Cytometry & Cell Sorting Shared Resource, the Preclinical Imaging Research Laboratory, Microscopy & Imaging Shared Resource, Tissue Culture & Biorepository for Cell Lines and Biofluids Shared Resource, Histopathology & Tissue, and Animal Core Facilities supported by NCI Cancer Center Support Grant and U.S. Public Health Service Grant 2P30-CA-51008 and 1 S10 RR 15768-01. This investigation was performed in part in a facility constructed with support from Research Facilities Improvement grant C06RR14567 from the National Center for Research Resources, NIH.

Supporting Information Available: AFM image of intact TfRscFv-LipA-p53 (scL-p53) complexes; higher magnification of an area of the H&E stained section from Figure 2E; enlarged version of Figure 2F; time lapse images of subcellular localization of 6FAM-ODN *in vitro*; and time-dependent changes in expression of MGMT and p53 related proteins. This material is available free of charge *via* the Internet at http://pubs.acs.org.

REFERENCES AND NOTES

1. Nagasawa, D. T.; Chow, F.; Yew, A.; Kim, W.; Cremer, N.; Yang, I. Temozolomide and Other Potential Agents for the Treatment of Glioblastoma Multiforme. *Neurosurg. Clin. North Am.* **2012**, *23*, 307–322.
2. Vredenburgh, J. J.; Desjardins, A.; Herndon, J. E., 2nd; Dowell, J. M.; Reardon, D. A.; Quinn, J. A.; Rich, J. N.; Sathornsumetee, S.; Gururangan, S.; Wagner, M.; *et al.* Phase II Trial of Bevacizumab and Irinotecan in Recurrent Malignant Glioma. *Clin. Cancer Res.* **2007**, *13*, 1253–1259.
3. Hou, L. C.; Veeravagu, A.; Hsu, A. R.; Tse, V. C. Recurrent Glioblastoma Multiforme: a Review of Natural History and Management Options. *Neurosurg. Focus* **2006**, *20*, E5.
4. Johannessen, T. C.; Bjerkvig, R.; Tysnes, B. B. DNA Repair and Cancer Stem-Like Cells—Potential Partners in Glioma Drug Resistance? *Cancer Treat. Rev.* **2008**, *34*, 558–567.
5. Chamberlain, M. C. Temozolomide: Therapeutic Limitations in the Treatment of Adult High-Grade Gliomas. *Expert Rev. Neurother.* **2010**, *10*, 1537–1544.
6. Ma, J.; Murphy, M.; O'Dwyer, P. J.; Berman, E.; Reed, K.; Gallo, J. M. Biochemical Changes Associated with a Multidrug-Resistant Phenotype of a Human Glioma Cell Line with Temozolomide-Acquired Resistance. *Biochem. Pharmacol.* **2002**, *63*, 1219–1228.
7. Fruehauf, J. P.; Brem, H.; Brem, S.; Sloan, A.; Barger, G.; Huang, W.; Parker, R. *In Vitro* Drug Response and Molecular Markers Associated with Drug Resistance in Malignant Gliomas. *Clin. Cancer Res.* **2006**, *12*, 4523–4532.
8. Bocangel, D.; Sengupta, S.; Mitra, S.; Bhakat, K. K. p53-Mediated Down-Regulation of the Human DNA Repair Gene O^6-Methylguanine-DNA Methyltransferase (MGMT) *via* Interaction with Sp1 Transcription Factor. *Anticancer Res.* **2009**, *29*, 3741–3750.
9. Quinn, J. A.; Desjardins, A.; Weingart, J.; Brem, H.; Dolan, M. E.; Delaney, S. M.; Vredenburgh, J.; Rich, J.; Friedman, A. H.; Reardon, D. A.; *et al.* Phase I Trial of Temozolomide Plus O^6-Benzylguanine for Patients with Recurrent or Progressive Malignant Glioma. *J. Clin. Oncol.* **2005**, *23*, 7178–7187.
10. Liu, L.; Gerson, S. L. Targeted Modulation of MGMT: Clinical Implications. *Clin. Cancer Res.* **2006**, *12*, 328–331.
11. Kanzawa, T.; Bedwell, J.; Kondo, Y.; Kondo, S.; Germano, I. M. Inhibition of DNA Repair for Sensitizing Resistant Glioma Cells to Temozolomide. *J. Neurosurg.* **2003**, *99*, 1047–1052.
12. Ohka, F.; Natsume, A.; Wakabayashi, T. Current Trends in Targeted Therapies for Glioblastoma Multiforme. *Neurol. Res. Int.* **2012**, *2012*, 878425.
13. Nagpal, J.; Jamoona, A.; Gulati, N. D.; Mohan, A.; Braun, A.; Murali, R.; Jhanwar-Uniyal, M. Revisiting the Role of p53 in Primary and Secondary Glioblastomas. *Anticancer Res.* **2006**, *26*, 4633–4639.
14. Zheng, H.; Ying, H.; Yan, H.; Kimmelman, A. C.; Hiller, D. J.; Chen, A. J.; Perry, S. R.; Tonon, G.; Chu, G. C.; Ding, Z.; *et al.* p53 and Pten Control Neural and Glioma Stem/Progenitor Cell Renewal and Differentiation. *Nature* **2008**, *455*, 1129–1133.
15. Ohgaki, H.; Dessen, P.; Jourde, B.; Horstmann, S.; Nishikawa, T.; Di Patre, P. L.; Burkhard, C.; Schuler, D.; Probst-Hensch, N. M.; Maiorka, P. C.; *et al.* Genetic Pathways to Glioblastoma: a Population-Based Study. *Cancer Res.* **2004**, *64*, 6892–6899.
16. Srivenugopal, K. S.; Shou, J.; Mullapudi, S. R.; Lang, F. F., Jr.; Rao, J. S.; Ali-Osman, F. Enforced Expression of Wild-Type p53 Curtails the Transcription of the O(6)-Methylguanine-DNA Methyltransferase Gene in Human Tumor Cells and Enhances Their Sensitivity to Alkylating Agents. *Clin. Cancer Res.* **2001**, *7*, 1398–1409.
17. Cerrato, J. A.; Yung, W. K.; Liu, T. J. Introduction of Mutant p53 into a Wild-Type p53-Expressing Glioma Cell Line Confers Sensitivity to Ad-p53-Induced Apoptosis. *Neuro-Oncol.* **2001**, *3*, 113–122.
18. Bobustuc, G. C.; Baker, C. H.; Limaye, A.; Jenkins, W. D.; Pearl, G.; Avgeropoulos, N. G.; Konduri, S. D. Levetiracetam Enhances p53-Mediated MGMT Inhibition and Sensitizes Glioblastoma Cells to Temozolomide. *Neuro-Oncol.* **2010**, *12*, 917–927.
19. Sato, A.; Sunayama, J.; Matsuda, K.; Seino, S.; Suzuki, K.; Watanabe, E.; Tachibana, K.; Tomiyama, A.; Kayama, T.; Kitanaka, C. MEK-ERK Signaling Dictates DNA-Repair Gene MGMT Expression and Temozolomide Resistance of Stem-Like Glioblastoma Cells *via* the MDM2-p53 Axis. *Stem Cells* **2011**, *29*, 1942–1951.
20. Daniels, T. R.; Bernabeu, E.; Rodríguez, J. A.; Patel, S.; Kozman, M.; Chiappetta, D. A.; Holler, E.; Ljubimova, J. Y.; Helguera, G.; Penichet, M. L. The Transferrin Receptor and the Targeted Delivery of Therapeutic Agents Against Cancer. *Biochim. Biophys. Acta* **2012**, *1820*, 291–317.
21. Xu, L.; Frederik, P.; Pirollo, K. F.; Tang, W. H.; Rait, A.; Xiang, L. M.; Huang, W.; Cruz, I.; Yin, Y.; Chang, E. H. Self-Assembly of a Virus-Mimicking Nanostructure System for Efficient Tumor-Targeted Gene Delivery. *Hum. Gene Ther.* **2002**, *13*, 469–481.
22. Xu, L.; Pirollo, K. F.; Tang, W. H.; Rait, A.; Chang, E. H. Transferrin-Liposome-Mediated Systemic p53 Gene Therapy in Combination with Radiation Results in Regression of Human Head and Neck Cancer Xenografts. *Hum. Gene Ther.* **1999**, *10*, 2941–2952.
23. Xu, L.; Tang, W. H.; Huang, C. C.; Alexander, W.; Xiang, L. M.; Pirollo, K. F.; Rait, A.; Chang, E. H. Systemic p53 Gene Therapy of Cancer with Immunolipoplexes Targeted by Anti-Transferrin Receptor scFv. *Mol. Med.* **2001**, *7*, 723–734.
24. Xu, L.; Huang, C. C.; Huang, W.; Tang, W. H.; Rait, A.; Yin, Y. Z.; Cruz, I.; Xiang, L. M.; Pirollo, K. F.; Chang, E. H. Systemic Tumor-Targeted Gene Delivery by Anti-Transferrin Receptor scFv-Immunoliposomes. *Mol. Cancer Ther.* **2002**, *1*, 337–346.
25. Pirollo, K. F.; Rait, A.; Zhou, Q.; Zhang, X. Q.; Zhou, J.; Kim, C. S.; Benedict, W. F.; Chang, E. H. Tumor-Targeting Nanocomplex Delivery of Novel Tumor Suppressor RB94 Chemosensitizes Bladder Carcinoma Cells *In Vitro* and *In Vivo*. *Clin. Cancer Res.* **2008**, *14*, 2190–2198.
26. Yu, W.; Pirollo, K. F.; Yu, B.; Rait, A.; Xiang, L.; Huang, W.; Zhou, Q.; Ertem, G.; Chang, E. H. Enhanced Transfection Efficiency of a Systemically Delivered Tumor-Targeting Immunolipoplex by Inclusion of a pH-Sensitive Histidylated Oligolysine Peptide. *Nucleic Acids Res.* **2004**, *32*, e48.
27. Pirollo, K. F.; Zon, G.; Rait, A.; Zhou, Q.; Yu, W.; Hogrefe, R.; Chang, E. H. Tumor-Targeting Nanoimmunoliposome Complex for Short Interfering RNA Delivery. *Hum. Gene Ther.* **2006**, *17*, 117–124.
28. Pirollo, K. F.; Rait, A.; Zhou, Q.; Hwang, S. H.; Dagata, J. A.; Zon, G.; Hogrefe, R. I.; Palchik, G.; Chang, E. H. Materializing the Potential of Small Interfering RNA *via* a Tumor-Targeting Nanodelivery System. *Cancer Res.* **2007**, *67*, 2938–2943.
29. Hwang, S. H.; Rait, A.; Pirollo, K. F.; Zhou, Q.; Yenugonda, V. M.; Chinigo, G. M.; Brown, M. L.; Chang, E. H. Tumor-

Targeting Nanodelivery Enhances the Anticancer Activity of a Novel Quinazolinone Analogue. *Mol. Cancer Ther.* **2008**, *7*, 559–568.
30. Senzer, N.; Nemunaitis, J.; Nemunaitis, D.; Bedell, C.; Edelman, G.; Barve, M.; Nunan, R.; Pirollo, K. F.; Rait, A.; Chang, E. H.; Phase, I. Study of a Systemically Delivered p53 Nanoparticle in Advanced Solid Tumors. *Mol. Ther.* **2013**, *21*, 1096–1103.
31. Nathanson, D.; Mischel, P. S. Charting the Course Across the Blood-Brain Barrier. *J. Clin. Invest.* **2011**, *121*, 31–33.
32. Kim, S. S.; Rait, A.; Rubab, F.; Rao, A. K.; Kiritsy, M. C.; Pirollo, K. F.; Wang, S.; Weiner, L. M.; Chang, E. H. The Clinical Potential of Targeted Nanomedicine: Delivering to Cancer Stem-Like Cells. *Mol. Ther.* **2014**, *22*, 278–291.
33. Dagata, J. A.; Farkas, N.; Dennis, C. L.; Shull, R. D.; Hackley, V. A.; Yang, C.; Pirollo, K. F.; Chang, E. H. Physical Characterization Methods for Iron Oxide Contrast Agents Encapsulated within a Targeted Liposome-Based Delivery System. *Nanotechnology* **2008**, *19*, 305101.
34. Farkas, N.; Dagata, J. A.; Yang, C.; Rait, A.; Pirollo, K. F.; Chang, E. H. Combined Scanning Probe and Light Scattering Characterization of Multi-Stage Self-Assembly of Targeted Liposome-Based Delivery Systems. *Meas. Sci. Technol.* **2011**, *22*, 024006.
35. Bajgai, M. P.; Aryal, S.; Lee, D. R.; Park, S.-J.; Kim, H. Y. Physicochemical Characterization of Self-Assembled Poly-(∈-caprolactone) Grafted Dextran Nanoparticles. *Colloid Polym. Sci.* **2008**, *286*, 517–524.
36. Tabatt, K.; Kneuer, C.; Sameti, M.; Olbrich, C.; Müller, R. H.; Lehr, C. M.; Bakowsky, U. Transfection with Different Colloidal Systems: Comparison of Solid Lipid Nanoparticles and Liposomes. *J. Controlled Release* **2004**, *97*, 321–332.
37. Nakano, K.; Tozuka, Y.; Yamamoto, H.; Kawashima, Y.; Takeuchi, H. A Novel Method for Measuring Rigidity of Submicron-Size Liposomes with Atomic Force Microscopy. *Int. J. Pharm.* **2008**, *355*, 203–209.
38. Gohy, J.-F.; Hofmeier, H.; Alexeev, A.; Schubert, U. S. Aqueous Micelles from Supramolecular Graft Copolymers. *Macromol. Chem. Phys.* **2003**, *204*, 1524–1530.
39. Thomson, N. H.; Collin, I.; Davies, M. C.; Palin, K.; Parkins, D.; Roberts, C. J.; Tendler, S. J. B.; Williams, P. M. Atomic Force Microscopy of Cationic Liposomes. *Langmuir* **2000**, *16*, 4813–4818.
40. Volcke, C.; Pirotton, S.; Grandfils, Ch.; Humbert, C.; Thiry, P. A.; Ydens, I.; Dubois, P.; Raes, M. Influence of DNA Condensation State on Transfection Efficiency in DNA/Polymer Complexes: An AFM and DLS Comparative Study. *J. Biotechnol.* **2006**, *125*, 11–21.
41. Guo, S.; Huang, L. Nanoparticles Escaping RES and Endosome: Challenges for siRNA Delivery for Cancer Therapy. *J. Nanomater.* **2011**, *2011*, 742895.
42. Hegi, M. E.; Diserens, A. C.; Gorlia, T.; Hamou, M. F.; de Tribolet, N.; Weller, M.; Kros, J. M.; Hainfellner, J. A.; Mason, W.; Mariani, L.; *et al.* MGMT Gene Silencing and Benefit from Temozolomide in Glioblastoma. *N. Engl. J. Med.* **2005**, *352*, 997–1003.
43. Kitange, G. J.; Carlson, B. L.; Mladek, A. C.; Decker, P. A.; Schroeder, M. A.; Wu, W.; Grogan, P. T.; Giannini, C.; Ballman, K. V.; Buckner, J. C.; *et al.* Evaluation of MGMT Promoter Methylation Status and Correlation with Temozolomide Response in Orthotopic Glioblastoma Xenograft Model. *J. Neurooncol.* **2009**, *92*, 23–31.
44. Martin, S.; Janouskova, H.; Dontenwill, M. Integrins and p53 Pathways in Glioblastoma Resistance to Temozolomide. *Front. Oncol.* **2012**, *2*, 157.
45. Carlson, B. L.; Grogan, P. T.; Mladek, A. C.; Schroeder, M. A.; Kitange, G. J.; Decker, P. A.; Giannini, C.; Wu, W.; Ballman, K. A.; James, C. D.; *et al.* Radiosensitizing Effects of Temozolomide Observed *In Vivo* only in a Subset of O^6-Methylguanine-DNA Methyltransferase Methylated Glioblastoma Multiforme Xenografts. *Int. J. Radiat. Oncol., Biol., Phys.* **2009**, *75*, 212–219.
46. Combs, S. E.; Rieken, S.; Wick, W.; Abdollahi, A.; von Deimling, A.; Debus, J.; Hartmann, C. Prognostic Significance of IDH-1 and MGMT in Patients with Glioblastoma: One Step Forward, and One Step Back? *Radiat. Oncol.* **2011**, *6*, 115.
47. Xu, G. W.; Mymryk, J. S.; Cairncross, J. G. Pharmaceutical-Mediated Inactivation of p53 Sensitizes U87MG Glioma Cells to BCNU and Temozolomide. *Int. J. Cancer* **2005**, *116*, 187–192.
48. Xu, G. W.; Mymryk, J. S.; Cairncross, J. G. Inactivation of p53 Sensitizes Astrocytic Glioma Cells to BCNU and Temozolomide, but not Cisplatin. *J. Neurooncol.* **2005**, *74*, 141–149.
49. Hirose, Y.; Berger, M. S.; Pieper, R. O. p53 Effects both the Duration of G2/M Arrest and the Fate of Temozolomide-Treated Human Glioblastoma Cells. *Cancer Res.* **2001**, *61*, 1957–1963.
50. Blough, M. D.; Beauchamp, D. C.; Westgate, M. R.; Kelly, J. J.; Cairncross, J. G. Effect of Aberrant p53 Function on Temozolomide Sensitivity of Glioma Cell Lines and Brain Tumor Initiating Cells from Glioblastoma. *J. Neurooncol.* **2011**, *102*, 1–7.
51. Hermisson, M.; Klumpp, A.; Wick, W.; Wischhusen, J.; Nagel, G.; Roos, W.; Kaina, B.; Weller, M. O^6-Methylguanine DNA Methyltransferase and p53 Status Predict Temozolomide Sensitivity in Human Malignant Glioma Cells. *J. Neurochem.* **2006**, *96*, 766–776.
52. Roos, W. P.; Batista, L. F.; Naumann, S. C.; Wick, W.; Weller, M.; Menck, C. F.; Kaina, B. Apoptosis in Malignant Glioma Cells Triggered by the Temozolomide-Induced DNA Lesion O^6-Methylguanine. *Oncogene* **2007**, *26*, 186–197.
53. Zhang, W. B.; Wang, Z.; Shu, F.; Jin, Y. H.; Liu, H. Y.; Wang, Q. J.; Yang, Y. Activation of AMP-Activated Protein Kinase by Temozolomide Contributes to Apoptosis in Glioblastoma Cells *via* p53 Activation and mTORC1 Inhibition. *J. Biol. Chem.* **2010**, *285*, 40461–40471.
54. Frosina, G. DNA Repair and Resistance of Gliomas to Chemotherapy and Radiotherapy. *Mol. Cancer Res.* **2009**, *7*, 989–999.
55. Dean, M.; Fojo, T.; Bates, S. Tumour Stem Cells and Drug Resistance. *Nat. Rev. Cancer* **2005**, *5*, 275–284.
56. Visvader, J. E.; Lindeman, G. J. Cancer Stem Cells in Solid Tumours: Accumulating Evidence and Unresolved Questions. *Nat. Rev. Cancer* **2008**, *8*, 755–768.
57. Eramo, A.; Ricci-Vitiani, L.; Zeuner, A.; Pallini, R.; Lotti, F.; Sette, G.; Pilozzi, E.; Larocca, L. M.; Peschle, C.; De Maria, R. Chemotherapy Resistance of Glioblastoma Stem Cells. *Cell Death Differ.* **2006**, *13*, 1238–1241.
58. Beier, D.; Schulz, J. B.; Beier, C. P. Chemoresistance of Glioblastoma Cancer Stem Cells—Much More Complex Than Expected. *Mol. Cancer* **2011**, *10*, 128.
59. Miaczynska, M.; Bar-Sagi, D. Signaling Endosomes: Seeing is Believing. *Curr. Opin. Cell Biol.* **2010**, *22*, 535–540.
60. Zbinden, M.; Duquet, A.; Lorente-Trigos, A.; Ngwabyt, S. N.; Borges, I.; Ruiz, i; Altaba, A. NANOG Regulates Glioma Stem Cells and is Essential *In Vivo* Acting in a Cross-Functional Network with GLI1 and p53. *EMBO J.* **2010**, *29*, 2659–2674.
61. Zheng, H.; Ying, H.; Yan, H.; Kimmelman, A. C.; Hiller, D. J.; Chen, A. J.; Perry, S. R.; Tonon, G.; Chu, G. C.; Ding, Z.; *et al.* Pten and p53 Converge on c-Myc to Control Differentiation, Self-Renewal, and Transformation of Normal and Neoplastic Stem Cells in Glioblastoma. *Cold Spring Harbor Symp. Quant. Biol.* **2008**, *73*, 427–437.
62. Jiang, G.; Wei, Z. P.; Pei, D. S.; Xin, Y.; Liu, Y. Q.; Zheng, J. N. A Novel Approach to Overcome Temozolomide Resistance in Glioma and Melanoma: Inactivation of MGMT by Gene Therapy. *Biochem. Biophys. Res. Commun.* **2011**, *406*, 311–314.
63. Tentori, L.; Graziani, G. Recent Approaches to Improve the Antitumor Efficacy of Temozolomide. *Curr. Med. Chem.* **2009**, *16*, 245–257.
64. Shah, G. D.; Socci, N. D.; Gold, J. S.; Wolchok, J. D.; Carvajal, R. D.; Panageas, K. S.; Viale, A.; Brady, M. S.; Coit, D. G.; Chapman, P. B. Phase II Trial of Neoadjuvant Temozolomide in Resectable Melanoma Patients. *Ann. Oncol.* **2010**, *21*, 1718–1722.
65. Patel, P. M.; Suciu, S.; Mortier, L.; Kruit, W. H.; Robert, C.; Schadendorf, D.; Trefzer, U.; Punt, C. J.; Dummer, R.; Davidson, N.; *et al.* Extended Schedule, Escalated Dose Temozolomide *Versus* Dacarbazine in Stage IV Melanoma: Final Results of a Randomised Phase III Study (EORTC 18032). *Eur. J. Cancer* **2011**, *47*, 1476–1483.

66. Laber, D. A.; Khan, M. I.; Kloecker, G. H.; Schonard, C.; Taft, B. S.; Salvador, C. A Phase I Study of Thalidomide, Capecitabine and Temozolomide in Advanced Cancer. *Cancer Biol. Ther.* **2007**, *6*, 840–845.
67. Chan, J. A.; Stuart, K.; Earle, C. C.; Clark, J. W.; Bhargava, P.; Miksad, R.; Blaszkowsky, L.; Enzinger, P. C.; Meyerhardt, J. A.; Zheng, H.; *et al.* Prospective Study of Bevacizumab Plus Temozolomide in Patients with Advanced Neuroendocrine Tumors. *J. Clin. Oncol.* **2012**, *30*, 2963–2968.
68. Siena, S.; Crino, L.; Danova, M.; Del Prete, S.; Cascinu, S.; Salvagni, S.; Schiavetto, I.; Vitali, M.; Bajetta, E. Dose-Dense Temozolomide Regimen for the Treatment of Brain Metastases from Melanoma, Breast Cancer, or Lung Cancer Not Amenable to Surgery or Radiosurgery: A Multicenter Phase II Study. *Ann. Oncol.* **2010**, *21*, 655–661.
69. Marosi, C. Complications of Chemotherapy in Neuro-Oncology. In *Handbook of Clinical Neurology*; Grisold, W., Soffietti, R., Eds.; Elsevier: New York, 2012; pp 873−885.
70. Gefen, N.; Brkic, G.; Galron, D.; Priel, E.; Ozer, J.; Benharroch, D.; Gopas, J. Acquired Resistance to 6-Thioguanine in Melanoma Cells Involves the Repair Enzyme O^6-Methylguanine-DNA Methyltransferase (MGMT). *Cancer Biol. Ther.* **2010**, *9*, 49–55.
71. Kokkinakis, D. M.; Ahmed, M. M.; Delgado, R.; Fruitwala, M. M.; Mohiuddin, M.; Albores-Saavedra, J. Role of O^6-Methylguanine-DNA Methyltransferase in the Resistance of Pancreatic Tumors to DNA Alkylating Agents. *Cancer Res.* **1997**, *57*, 5360–5368.
72. Kulke, M. H.; Hornick, J. L.; Frauenhoffer, C.; Hooshmand, S.; Ryan, D. P.; Enzinger, P. C.; Meyerhardt, J. A.; Clark, J. W.; Stuart, K.; Fuchs, C. S.; *et al.* O^6-Methylguanine DNA Methyltransferase Deficiency and Response to Temozolomide-Based Therapy in Patients with Neuroendocrine Tumors. *Clin. Cancer Res.* **2009**, *15*, 338–345.
73. Badie, B.; Goh, C. S.; Klaver, J.; Herweijer, H.; Boothman, D. A. Combined Radiation and p53 Gene Therapy of Malignant Glioma Cells. *Cancer Gene Ther.* **1999**, *6*, 155–162.
74. Bahr, O.; Wick, W.; Weller, M. Modulation of MDR/MRP by Wild-Type and Mutant p53. *J. Clin. Invest.* **2001**, *107*, 643–646.
75. Teicher, B. A.; Menon, K.; Alvarez, E.; Galbreath, E.; Shih, C.; Faul, M. Antiangiogenic and Antitumor Effects of a Protein Kinase Cbeta Inhibitor in Human T98G Glioblastoma Multiforme Xenografts. *Clin. Cancer Res.* **2001**, *7*, 634–640.